TALLINN UNIVERSITY OF TECHNOLOGY
SCHOOL OF ENGINEERING
Department of Chemical and Materials Engineering

Post deposition annealing effect on properties of chemically deposited CdS films and performance of CdS/Sb_2Se_3 solar cells

Lõõmutamise mõju järeltöötlusena keemiliselt sadestatud CdS kilede omadustele ja CdS/Sb_2Se_3 päikesepatareide tõhususele

MASTER THESIS

Student: Madhawa Basnayaka

Student code: 184647KAYM

Supervisor: Dr. Nicolae Spalatu

Tallinn 2021

AUTHOR'S DECLARATION

Hereby I declare that I have written this thesis independently.
No academic degree has been applied for based on this material. All works, major viewpoints and data of the other authors used in this thesis have been referenced.

"20" May 2021

Author: Madhawa Basnayaka
/signature /

Thesis is in accordance with terms and requirements

"....." ..... 20….

Supervisor: ….....
/signature/

Accepted for defense

"....."..... 20….

Chairman of theses defence commission: .....
/name and signature/

Department of Chemical and Materials Engineering

THESIS TASK

Student: Madhawa Basnayaka, 184647KAYM

Study programme: Materials and Processes of sustainable Energetics

Main specialty: Materials for sustainable energetic.

Supervisor: Dr. Nicolae Spalatu

Thesis topic:

In English Post deposition annealing effect on properties of chemically deposited CdS films and performance of CdS/Sb_2Se_3 solarcells.

In Estonian Lõõmutamise mõju järeltöötlusena keemiliselt sadestatud CdS kilede omadustele ja CdS/Sb_2Se_3 päikesepatareide tõhususele

Thesis main objectives:

1. To gain the knowledge and experiences in CBD CdS deposition parameters and post deposition treatments.
2. To study the impact annealing conditions and annealing temperature on the properties of CBD CdS thin films.
3. To familiarize with CSS method for fabrication of Sb_2Se_3 thin film solar cells.
4. To study the interrelation between annealing condition and annealing temperature on the performance of glass/FTO/CdS/Sb_2Se_3 solar cell device.
5. To get hand on experiences in thin film characterization and to acquire knowledge of the main principles of solar cells.

Thesis tasks and time schedule:

No	Task description	Deadline
1.	Deposition of CdS by chemical bath deposition on glass and FTO/glass substrates	
2.	Annealing of CBD CdS films on glass and FTO/glass substrates, in different conditions at different temperatures.	
3.	Deposition of Sb_2Se_3 absorber layer by CSS	
4.	Conducting material characterization methods for annealed CBD CdS layers.	
5.	Evaluate solar cell device performance by device characterization methods.	

Language: English **Deadline for submission of thesis:** "26th"May2021

Student: Madhawa Basnayaka "....."……..201….a

/signature/

Supervisor: Nicolae Spalatu ……"....."…….201….a

/signature/

Consultant: …… ….…… "....."…….201….a

/signature/

Head of study programme: ……..……

"....."……..201.a

/signature/

Table of Content

List of figures

List of Tables

PREFACE

Dr. Nicolae Spalatu proposed the thesis topic and primary thesis works centralized in the Laboratory of Thin Film Chemical Technologies. Through the research project, I was supported by Dr. Nicolae Spalatu, Dr. Atanas Katerski, Dr. Olga Volobujeva, Ph.D. students Robert Krautmann, and Sajeesh V.G.

The project was carried out for more than 1.5 years in 5 steps; depositing CdS on glass substrates using CBD method/Characterization of CBD CdS deposited on glass substrates/depositing CdS on FTO glass using CBD/depositing Sb_2Se_3 by CSS on annealed CBD CdS/making solar cell device and device characterization. Seeking a sustainable energy source as a teenager, my attention was captured by solar cells. My thanks go to Dr. Ilona Oja Acik and the Director of Materials and Environmental Technology Department, Dr. Malle Krunks, for providing facilities to fabricate solar cells and get professional experiences in working with characteristics equipment. The guidance and support I had from Prof. Sergei Bereznev as the program director is also remarkable. Special mention is Dr. Atanas Katerski, who has helped me technically and theoretically during the research project. This study was funded by the Estonian Research Council project PRG627 "Antimony chalcogenide thin films for next-generation semi-transparent solar cells applicable in electricity producing windows", the Estonian Research Council project PSG689 "Bismuth Chalcogenide Thin-Film Disruptive Green Solar Technology for Next Generation Photovoltaics", the Estonian Centre of Excellence project TK141 (TAR16016EK) "Advanced materials and high-technology devices for energy recuperation system", and the EU H2020 program under the ERA Chair project 5GSOLAR grant agreement No 952509.

The project can be divided in to two parts; during the first part, I presented how annealing conditions and annealing temperature affect the CBD CdS structural, optical, electrical properties by characterizing the film properties (UV–vis spectroscopy, bandgap calculation, XRD measurement, crystallographic analysis, Van der Paw measurements) and, the major part of writing. In the next stage is the demonstration of how this annealing condition affects the glass/FTO/CBD–CdS/CSS Sb_2Se_3solar cell device mainly on efficiency, open–circuit voltage (V_{OC}), short circuit current density (J_{SC}), and fill factor (FF). I found an optimal temperature where the buffer layer CBD CdS on glass substrates shows better performance. Glass/FTO/CBD–CdS/CSS Sb_2Se_3 solar cell achieved photo conversion efficiency of 2.8%, which was fabricated using CBD CdS annealed in air at 200°C.

Keywords: chemical bath deposition, close–spaced sublimation, thin film solar cells, antimony seleenide, cadmium sulfide.

List of abbreviations and symbols

CBD	Chemical bath deposition
CdS	Cadmium Sulfide
Sb_2Se_3	Antimony selenide
PV	Photovoltaics
CdTe	Cadmium telluride
CIGS	Cadmium indium gallium Selenide
CSS	Closed spaced sublimation
CZTS	Cu_2ZnSnS_4
E_g	Optical bandgap
FF	Fill factor
FTO	Fluorine doped tin oxide
ITO	Indium tin oxide
J_{SC}	Short–circuit current
V_{OC}	Open circuit voltage
PVD	Physical vapor deposition
EQE	External quantum efficiency
SEM	Scanning electron microscopy
XRD	X–ray diffraction
STC	Standard test condition
SC	Semiconductors
EQE	External Quantum Efficiency

INTRODUCTION

We are living in year 2021, when terms like "global warming," "climate change," "carbon footprint" have become our common vocabulary. The recent global pandemic arouses the seriousness of climate change. Out of many other environmentally hazardous human activities, fossil fuel usage has been the leading. Globally, we are driving to renewable energies, but 80% of energy is coming from fossil fuel[1]. The sun is the most consistent and reliable energy source, with the surface intensity of solar radiation is about 6.33x107W/m^2. The solar constant (ISC) is the average solar radiation incident on an imaginary surface near 1367 W/m^2[2]. Undoubtedly solar energy is the most abundant renewable energy source with the highest potential to provide the global energy requirement. A combination of p–type and n–type semiconductors is called the p–n junction, the base of photovoltaic cells, which convert solar energy directly to electricity without any environmentally harmful outputs.

Under the STC (Standard Test Conditions) 1000W irradiance, air mass 1.5 light spectrums and 298K device temperature, following solar cells has recorded some remarkable efficiencies; iii – v multi–junction solar cells 47.1%, monocrystalline–Si 26.7%, CIGS (Copper Indium Gallium Selenide) 23.4%, multi–crystalline– Si 23.2% and, CdTe 21%[3].

In the past 20 years, CdTe based and CIGS based solar cells have been improving significantly with a common factor of CdS as the buffer film which, plays a major role in recent past achievements. Many reports show that $CdCl_2$ treatment on CdS buffer layer is very beneficial for CdS/CdTe and CdS/Sb_2Se_3 solar cells, which provide grain growth and passivate grain boundaries[4].

In CdS/Sb_2Se_3 solar cells, the crystallization and morphology of the Sb_2Se_3 absorber layer are strongly affected by the deposition of the CdS buffer layer and the crystalline structure of CdS on the TCO (Transparent Conductive Oxide) substrates[5]. Furthermore, the intermixing of CdS/ Sb_2Se_3 is a lot reliant on the properties of the CdS layers. CdS pre–treatments are carried out to restructure the CdS and sharpen the transmission edge, obviously intended to restrict intermixing by expanding the grain size.

The chemical bath deposition (CBD) method provides very thin, uniform, compact, and adherent thin films for an ideal behaviour on solar cell devices. CBD is a low cost but proper technique proceeds at low temperature. Adequate post–deposition thermal treatment must take place for re–crystallization of the CdS thin films. CBD process is carried out in the aqueous medium, which results in a significant contribution of oxygen and hydrogen compounds to the growth mechanism of CdS

furthermore on the properties of CdS thin films. Previously, many studies have been performed to find out the chemical process during the deposition in the wake of the ordinary properties change of CdS. The OH group features in the S^{-2} site in the CdS lattice; it acts as a donor dopant that considerably modified CdS thin films' properties[6]. During the post–deposition thermal treatment, OH compound and other impurities will be removed, but properties electrical, structural and optical properties will be influenced.

The objective of this study is the streamlining of CdS thin films which are improved by post–deposition treatment for application in Sb_2Se_3 solar cell. CBD CdS thin films were treated in air and vacuum, from 200°C to 400°C, for 30 minutes.

The thesis is alienated into three chapters. Chapter 1 contains the literature overview describing the main properties of CBD CdS thin films and solar cells based on a Sb_2Se_3 absorber with CBD CdS as the buffer layer.

In chapter 2, the discussion concentrated about the preparation of CBD CdS thin films, annealing and characterization methods. In chapter 3 briefly discuss the prepared CBD CdS film properties and the application of CBD CdS annealed in two contrasting conditions, air and vacuum, at different temperatures in solar cell devices.

1. LITERATURE OVERVIEW

1.1 Thin film solar cells

1.1.1 The thin film industry

In definition, a thin film is referred to as a thin layer of material, including metallic, organic, or inorganic, whose thickness is in the range of few nanometers to few micrometers[7]. Moreover, thin films are two–dimensional nanostructures. In the fast–developing technological world, the thin–film industry is emerging as a more promising tool with its sophisticated properties. Thereby, it is being employed in several different sectors to overcome drawbacks in conventional methodologies and provide more enhanced uses for their consumers.

Among such various industries, the electronic industry is one of the dominant fields in which thin–film technology is widely employed. Thin–film technology plays a significant role in fulfilling the necessity of small–scale productions and low–volume productions to achieve a high–speed working capacity. There is a wide range of applications of thin films in the electronic industry, such as solar cells, light–emitting diodes (LED), actuators, displays, transponders, thin–film transistors, and memory devices [8]. However, the modern electronic industry of the world is getting deviated from the conventional rigid silicon chips, and it is heading more towards flexible electronics. Accordingly, some of the modern–day applications of thin films in the electronic industry are near–field communication (NFC), RFID (Radio Frequency Identification), brand protection tags, sensors, wearable, flexible displays, integrated solutions [9].

1.1.2 p–n junction of thin–film solar cell

The P–n junction is created when p–type semiconductor material and n–type semiconductor materials are brought together.

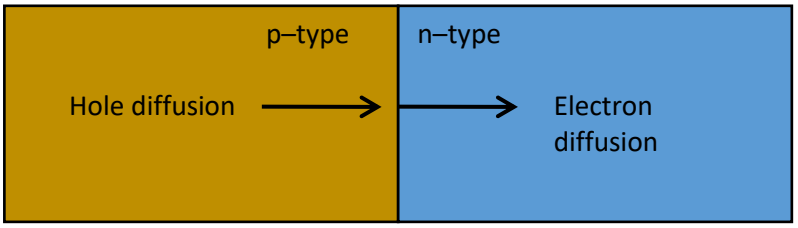

Figure 1. 1 Schematic view of majority carrier flow in p–n junction

The majority carriers' electron in n–type semiconductor diffuses to the p–type while

creating minority carriers' hole in an n–type semiconductor. As a result of that, the "depletion region" is created, which is vital in solar cells where no carriers can be found as well as acting as a potential barrier to the further diffusion of majority carriers with an internal electric field creating inside the depletion region that assure the charge separation in the p–n junction.

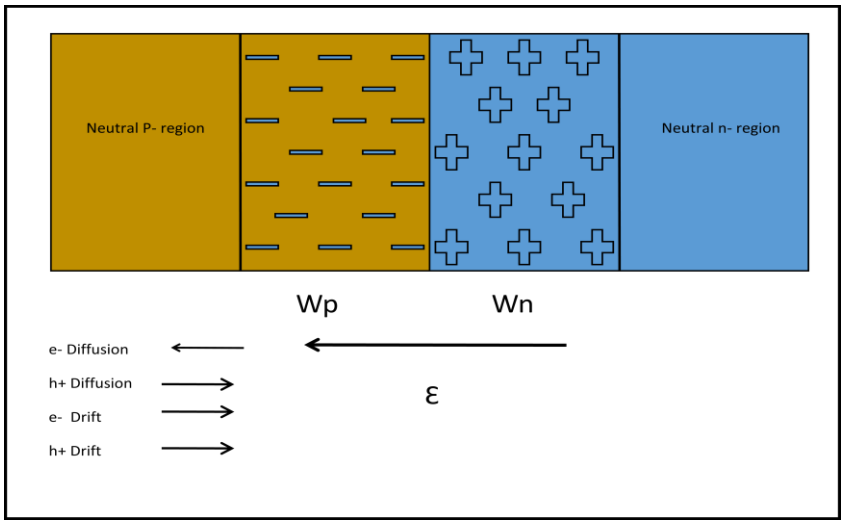

Figure 1. 2 Arrangement of depletion region in a p–n junction

There are three regions that can be distinguished in figure 1.2. On the p side, the material is neutral, and the band is flat figure 1.3[10]. On the n side, the material is neutral, and the band also flat. The most significant region is the depletion region where the bands are bent as well as an electrical field exists. Electron or hole entering the depletion region are drifted away. Thus, once equilibrium is established, a drift current exists that counterbalances the diffusion current[11]. Thin–film solar cell electron–hole pair generation takes place mainly in the base and the absorber side; thus, it is desired to have an extended depletion region towards the p–type absorber.

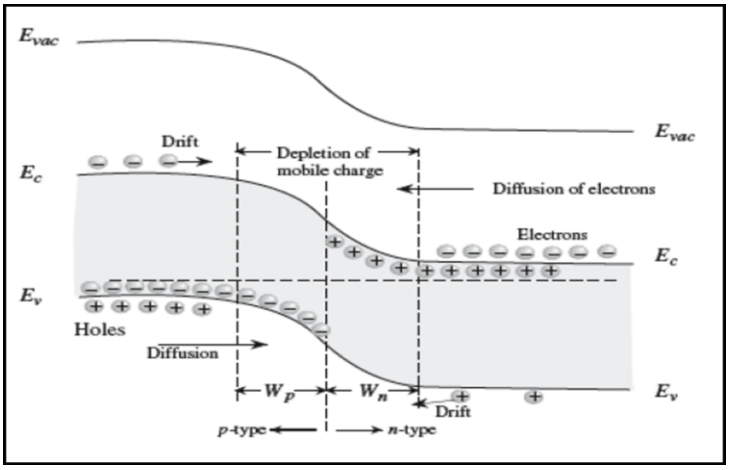

Figure 1. 3 Schematic of p–n junction with energy levels

To have the desired depletion region following requirement should be fulfilled, N_D– donor density>> N_A –acceptor density. Then the W_p becomes more comprehensive, and W_n becomes smaller. When the N_A >>N_D precisely, the opposite takes place.

1.1.3 Photo carrier generation, charge separation, and recombination

Solar cells convert the light energy of photons into electric current when photons collide with a suitable semiconductor device, when photons strike the solar cell, three probable scenarios can take place,

- The semiconductor materials will absorb–Photon
- Photons will be reflected off from the SC surface.
- The semiconductor material will absorb photons if the bandgap energy is less than photons' energy and generate electron–hole pairs.

Before photon transfers the energy to the electron, an electron in the valence band and electron "excites" by the energy given by photon to the conduction band where electrons can freely move around in the SC. Once the electron moved to the conduction band, it creates a "hole" in the valence band where the electron was previously part of covalent bonds. This hole empowers to move, bonded electrons nearby creating another hole leading to propagating holes throughout the lattice figure 1.4[10].

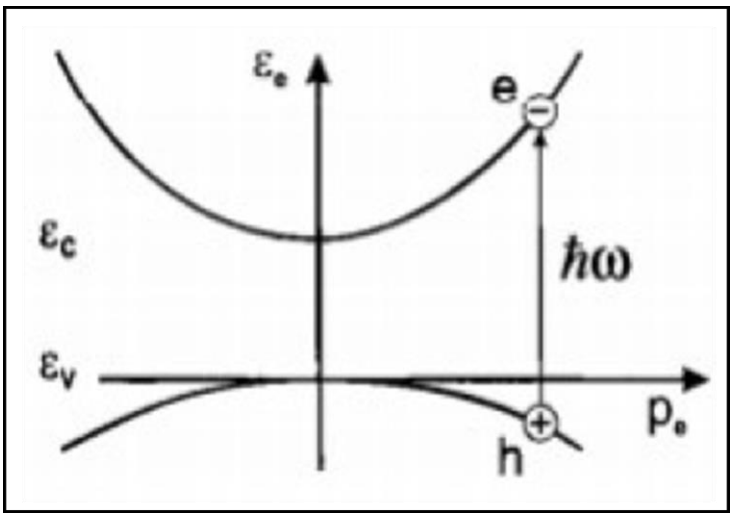

Figure 1. 4 Propagation of electron to conduction band and hole into valence band by the absorption of photon energy

According to section 1.2.1 and figure 1.2, there are two possibilities if the photo carriers are generated inside the depletion region, electrical field drives electron to the n–type and hole to the p–type material. If the generation takes place outside the depletion region, the pair should reach the depletion region to prevent the recombination with the majority carriers.

The generation point is a crucial factor; the distance of electrons generated from the depletion region is called diffusion length (L_D) figure 1.4. If the generation point> L_D, then they will be lost to recombination while within the distance L_D is separated from the hole at the junction successfully[12].

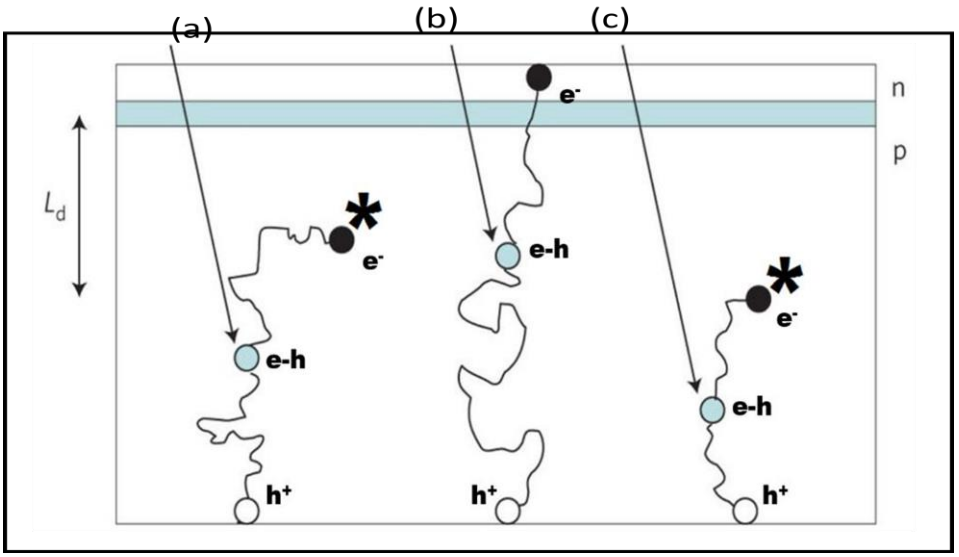

Figure 1. 5 Minority carrier diffusion to the depletion region. a,b> LD do not make to the depletion region. c< LD will make to the depletion region

Recombination is the opposite of the generation process. In other words, the

recombination process wipes out the generated e–h pairs. The following table provides the summary of the recombination processes which can be identified in thin films,

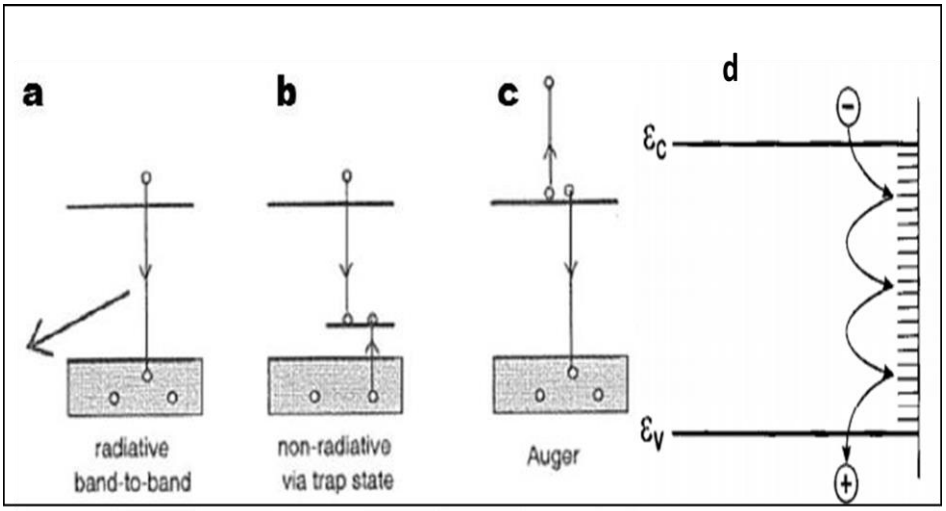

Figure 1. 6 (a) Radiative recombination (b) SRH recombination, (c) Auger recombination, and (d) Surface recombination [18][16]

1.1.4 Configuration of thin–film solar cell

Mainly there are two types of configurations: superstrate configuration, in which lights enter through the glass substrates, while in the substrate configuration, light enters through the last layer to be deposited. The main components of thin–film solar cells can be listed as follows. There are four primary recombination and summaries

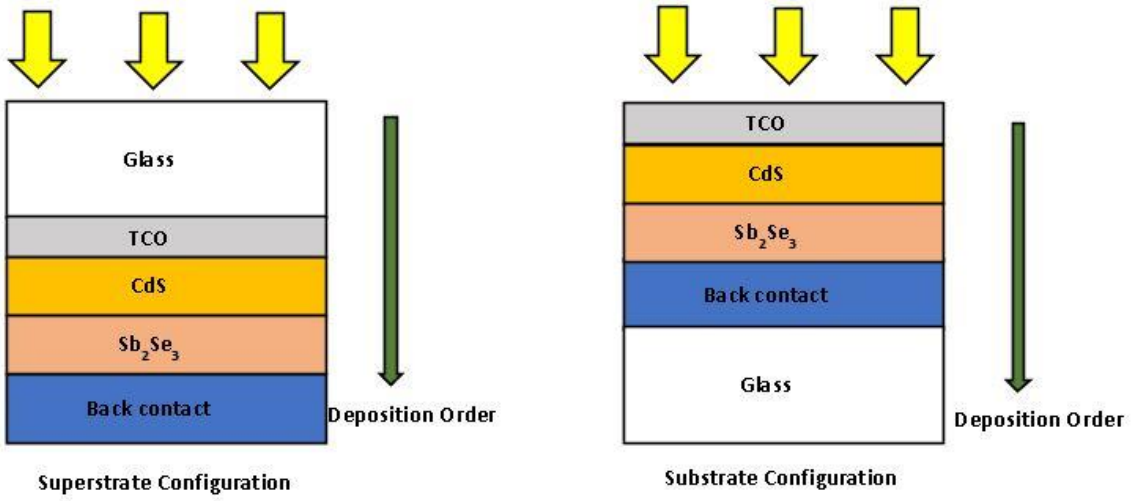

Figure 1. 7 Schematic cross section of the thin film solar cell configuration

p–type material: Majority carriers are holes with high absorption coefficient and low bandgap energy.

n–type material: Buffer or buffer layer with the majority carriers is electrons with low absorption coefficient and high bandgap energy. Generally, the buffer layer is transparent and conductive.

Substrate: Depend on the configuration type can be transparent or not materials like glass, metals, ceramic, or polymers.

Back contact: Materials which has higher conductivity to collect current as much as possible. Gold, Copper, Nickel, or Aluminum. Metal contact is supporting to extract photo carriers into the external circuit. Back contact is decided according to the working function (preferred to have a lower work function than the n–type SC). When the metal contact and the n–type semiconductor are brought together depletion region is created. But this region only confines to the n–type SC as the electron density of the metal is high.

Front contact: This must be conductive but transparent. Usually, transparent conductive oxides (TCO) such as fluorine doped tin oxide (FTO), indium tin oxide (ITO) or zinc oxide. Front contact is supporting extracting photo carriers into the external circuit. Similarly, p–type SC makes good ohmic contact with a metal which has a significant working function.

1.2 Varietal thin film preparation technique

High film homogeneity, low electrical resistivity, and high transparency in the visible region are required characteristics for the material intended to be used in the thin films. These properties are strongly dependent upon the deposition process. According to the deposition process, the grain size and the surface roughness would change. The film composition, crystal phase, and orientation, film thickness, and microstructure are the basic properties of the film, and these can be controlled by the deposition conditions [13].

There are numerous types of thin film deposition techniques already in practice, as depicted in the above diagram. Among those various techniques, the chemical deposition technique is being used on a large scale because of its low cost and ability to operate at low temperatures.

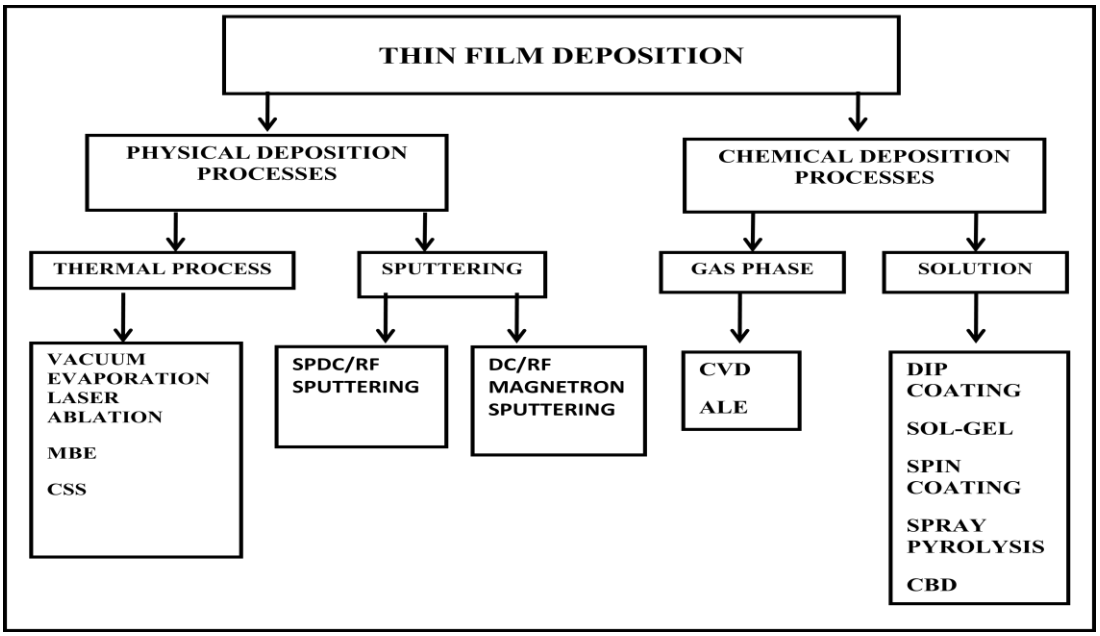

Figure 1. 8 Thin films deposition methods

Following methods have been used to prepare CdS thin films: Physical vapor deposition (PVD), radio frequency (RF) sputtering, close–spaced sublimation (CSS), pulsed laser evaporation, screen printing, electro deposition, CBD, spray pyrolysis, and metal–organic chemical vapor deposition.

1.2.1 Chemical Bath Deposition

The first reported compound semiconductor films formed by CBD included PbS, SbS and CuS were reported by Mokrushin in 1961[14].CdS polycrystalline thin films have very wide of reach, electroluminescent materials, field–effect transistors, light–emitting diodes, and especially in $CuIn_xGa_{1-x}Se_2$ (CIGS) and CdTe thin–film solar cells, respectively as a buffer layer and buffer layer materials [15], [16]. CBD has many positive outcomes; simple, low cost, and uniform large–area thin films due to inadequate processing temperature close to the room temperature. The fundamental necessity for as–prepared CdS thin films as the buffer layer of the CIGS or the buffer layer of the CdTe solar cell have been recorded as follows:

- The bandgap (E_g) value should be higher than possible. However, the buffer layer and absorber layer conduction band edge balance values are suitable.
- The thickness of the film must be very appropriate; high thickness will reduce photons reaching the absorber layer while too thin films prevent smooth films.
- The interface lattice should be as similar as possible.

- Electrical conductivity and optical conductivity should higher while reducing the defects[17].

The deposition mechanism of CBD CdS is based on the rate of releasing aqueous Cd^{+2} and S^{-2} ions and sequent condensation of these ions on the substrate [14]. The setup, as seen in figure1.9[18] of CBD consists of magnetic stirrer with a temperature controller and stirring rate, a thermometer to identify the bath temperature, magnets, and a solution container with a glass holder. The deposition of CdS films is done utilizing an alkaline aqueous arrangement made predominantly out of a Cd salt ($CdCl_2$, $CdSO_4$, CdI_2 etc.), thiourea ($SC(NH_2)_2$) as the sulfur source, and alkali (NH_3) as the complexing specialist. The arrangement of CdS happens heterogeneously on the substrate surface or homogeneously in the solution because of the unconstrained precipitation CdS in the form of secondary particles[19]. The parameters of CBD deposition as follows, the temperature, pH value, reactant concentration, composition of the solution and CBD time. The growth mechanism of CdS thin films can be categorized mainly from the microscopic point of view, ion–by–ion, cluster– by– cluster figure 1.10[20],complex decomposition cluster mechanism, and complex decomposition ion–by–ion mechanism[17], however the quality and the properties of the film based on the growth mechanism.

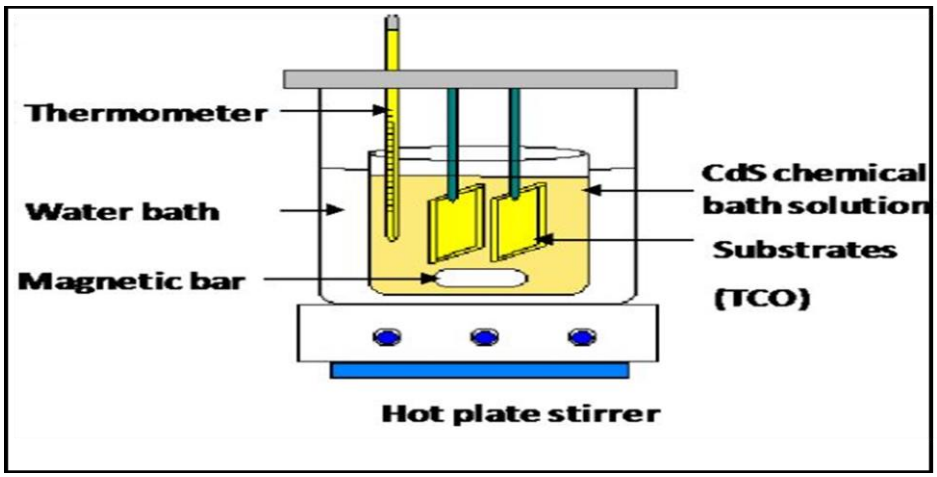

Figure 1. 9 Apparatus set up for CBD

The CdS growth mechanism can be categorized into three different stages according to the description by Lincot[21].

1. The reversible adsorption of cadmium hydroxide species, as shown in the equation1.1.

$$\mathbf{Cd(NH_3)^{2+}_4 + 2OH^- + Site \leftrightarrow Cd(OH)_2 + 4NH_3} \qquad \mathbf{1.1}$$

A complexing agent, which is ammonia (NH_3), is used to maintain Cd^{+2} ions to prevent it from precipitating as hydroxide and makes the bath alkaline.

2. Formation of a surface complex with thiourea. As shown in equation 1.2

$$\boldsymbol{Cd(OH)_2 + S = C(NH_2)_2 \rightarrow [(Cd(S = C(NH_2)_2)(OH_2)]} \qquad 1.\ 2$$

3. Formation of a surface complex with thiourea, as shown in the equation 1.3

$$\boldsymbol{[(Cd(S = C(NH_2)_2)(OH_2)] \rightarrow CdS + CN_2H_2 + 2H_2O + Site} \qquad 1.3$$

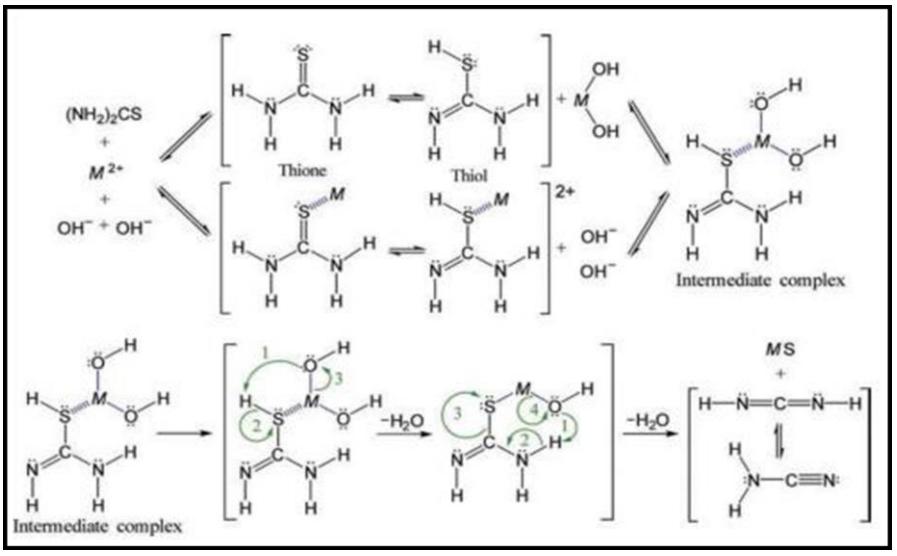

Figure 1. 10 Chemical representation of complex decomposition (Cluster mechanism)

The following reaction gives the summary reaction between ions of the cadmium–ammonia complex and thiourea molecules in ammonical solution.

$$\boldsymbol{Cd(NH_3)^{2+}_4 + SC(NH_2)_2 + 2OH^- \rightarrow CdS + CN_2H_2 + 2H_2O + Site} \qquad 1.\ 4$$

Out of all the parameters, temperature stands prominently for the epitaxial growth process of crystalline CdS[21]. The deposition will take place at a specific temperature, and a slight increase of temperature will multiply the growth rate at an alarming rate. The molar concentration of the bath solution for CdS can fluctuate over a working range. Each research group utilizes its particular formula, so there are, however, many combinations to deposit CdS as a research group working in the CBD CdS. The complexing agents like ammonia are added to the bath to slow down

the chemical reactions to maintain the slow release of Cd^{+2} and S^{-2} ions. However, few other significant parameters of the post–deposition process of CBD CdS likewise unequivocally impact the thin film properties.

1.2.2 Close Spaced Sublimation (CSS)

Close spaced sublimation (CSS) has a high deposition rate and idyllic for the bulky scale manufacturing thin films as CSS can be used to deposit solid materials on to the substrates in high vacuum easily; thus, the method has been used coating semiconductor materials with the boiling temperature less than 800°C[22]. Apart from the simplicity, CSS is the fastest technique of fabrications; for instance, CdTe (1–10μm) can be coated within 10minutes at the temperature of 600°C[22]. CSS is a method in which the solid transforms into vapor at high temperatures in a vacuum. The deposition on the substrate will get into a symmetrical position if the source and the substrate temperature are identical. Thus, the film thickness will prevent growing [23]. Impurities have become a key concern in thin–film fabrication, but CSS has the advantage of reducing the number of impurities in the film. By changing parameters like spacing between the source and the substrate, substrate temperature, source temperature, the composition of the source material, and vacuum pressure, we can easily control the quality of the thin film[24]figure 1.11[25].

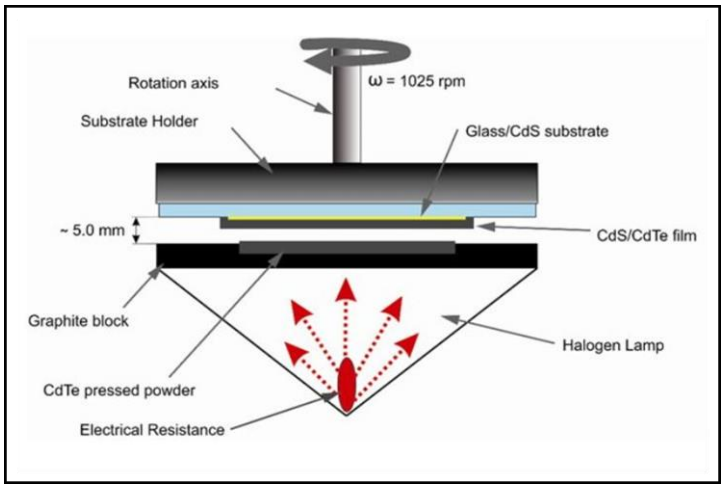

Figure 1. 11 CSS schematic view

The CSS setup consists of a quartz tube reinforced by a reactor, halogen lamps as the heating elements, thermocouples, and PID controllers to control the temperatures of the source and the substrate. The environment for the deposition is set up into a high vacuum in the reaction chamber by changing the rotary oil pump pressure to 10^{-4}Torr and the diffusion pump pressure in the range of 10^{-6}Torr. The

source and the substrates are kept at a distance where no mass loss takes place during vaporization. Once the vacuum is set up inside the chamber, the source starts to heat up until it reaches its vaporization temperature; meanwhile, the substrate is also heated up lower to the source temperature to the continuity of the process. To prevent any contamination or impurities participation, the chamber maintains at a high vacuum, and reaction chamber walls are also covered with quartz[26]. In general, for Sb_2Se_3 deposition, the pressure was maintained between 1–30 Torr, the substrate temperature was 500–600°C, and the source temperature was 700–800°C.

1.3 CdS as a buffer layer in thin film solar cells

1.3.1 Cadmium Sulfide

Cadmium sulfide (CdS) is an n type semiconductor of chemical compound that has the molecular formula of CdS. Phenotypically, it is yellow, and physically it is a semiconductor of electricity and insoluble in hot and cold water[27]. CdS exist as two different polymorphs. Namely, the hexagonal wurtzite which is textured in the [002] orientation and the cubic zinc blended structure which grows perpendicular to the (111) plane with lattice parameters a=5.825Å, b=4.136Å and c=6.716Å [28]. Furthermore, CdS is in the II–IV group with a direct bandgap of 2.42eV at room temperature. It has a molecular weight of 144.47gmol^{-1}, a high melting point of 1750°C, and a density of 4.826gcm^{-3}[29]. Higher bandgap energy and electrical properties suit solar cell applications as the buffer layer. It has many other applications in optoelectronic devices like a light–emitting diode, detectors, gas sensors, etc.

CdS nanostructures have got very prominent chemical, physical, optical, and electrical properties. CdS is a nano crystalline belonging to the cadmium chalcogenide family, and it is frequently used as the buffer layer material of CdS/CdTe in solar cells. The soluble bandgap, stability, and absorption coefficient in the visible range of the solar spectrum qualify for more intense applications of CdS nanostructures in solar cells. At room temperature CdS resistivity varies from $10^{-3}\Omega$.cm to $10^{8}\Omega$.cm and the specific conductivity is approximately $10^{-7}\Omega^{-1}cm^{-1}$[30]. CdS has hole's mobility 48cm^2/ (V.s) and electron's mobility 2.42.10^3 cm^2/ (V.s) in room temperature [31].

1.3.2 Post deposition treatments on CBD CdS thin films

As–deposited CdS thin films have shown poor crystalline properties, while annealing or post–treated thin films have shown better crystalline qualities. One major problem in as–deposited CdS thin films is, high concentration of contaminations and various particulates of homogeneously nucleated CdS[32], [33]. The structural and properties of CdS thin films were changed drastically by the presence of these impurities with supplies a layer with rapid speed recrystallization at low temperature [33], [34]. These highlights show the importance of post–deposition treatments to improve the properties of CdS thin films. By and large, the impacts of the annealing CBD CdS thin films are as per the following.

- Remove random strain and enhance the crystalline quality [35].
- Phase transition and, as a result, change the bandgap energy [10].
- Electrical properties are improved.

The influence of post–deposition treatments has been studied CBD CdS thin films by changing the annealing temperature, annealing duration, or the annealing atmosphere whether it's neutral, reducing, or oxidizing.

Moreover, independently of the deposition parameters, impurities can exist, for instance, nitrogen–related contaminants (up to 5 atomic%), but they can reduce by controlling the concentration of thiourea in the bath dissolving in water at 60°C[36]. However, the main impurity of CBD CdS is oxygen, and S site is substituted by oxygen, and Cd:S ratio is disrupted. There are many ways to regulate the oxygen impurities in sulfur sites, such as controlling deposition parameters, but here our main deliberation is removing impurities by thermal annealing.

1.4 Sb_2Se_3 as a novel PV absorber material

1.4.1 Properties of Sb_2Se_3

Polycrystalline and monocrystalline Si solar cells are at the top in mass production, almost 93% by 2016. Currently, researches and implementations are going on for alternative materials like CIGS, CdTe, and organic–inorganic hybrid perovskites because of their lightweight and flexibility. So far, they have achieved an overall efficiency of 20% on the lab scale[37]. Furthermore, CdTe and CIGS materials have primary constraints concerning mass–scale production. Sb_2Se_3 has become one of the promising candidates for the absorber layer as it is low toxic, low cost, high absorption coefficient($\alpha > 10^5$ cm^{-1})[37], suitable bandgap(~1.1eV), and contributes

to high–efficiency solar cells. Sb_2Se_3 is a binary compound with a single–phase which has a low melting point of (608˚C) with high vapor pressure guiding high–quality crystalline films production at low temperature(350˚C)[37]. Unlike GaAs, CdTe, and CIGS , which have 3–D crystal structure[38], Sb_2Se_3 possesses one dimensional (1–D) crystal structure. The crystal structure of Sb_2Se_3 is $(Sb_2Se_3)_n$ ribbons pack along the [001] direction through strong covalent bonds among Sb–Se atoms, whereas Van der Waals forces help to stack $(Sb_2Se_3)_n$ ribbons in [100] and [010] directions[38]. The main concern is the performance of polycrystalline PV materials is the non–radiative recombination losses. Sb_2Se_3 one dimensional crystal structure amusingly Van der Waals forces prevent the development of dangling bonds at the grain boundaries[38]figure 1.12[25].

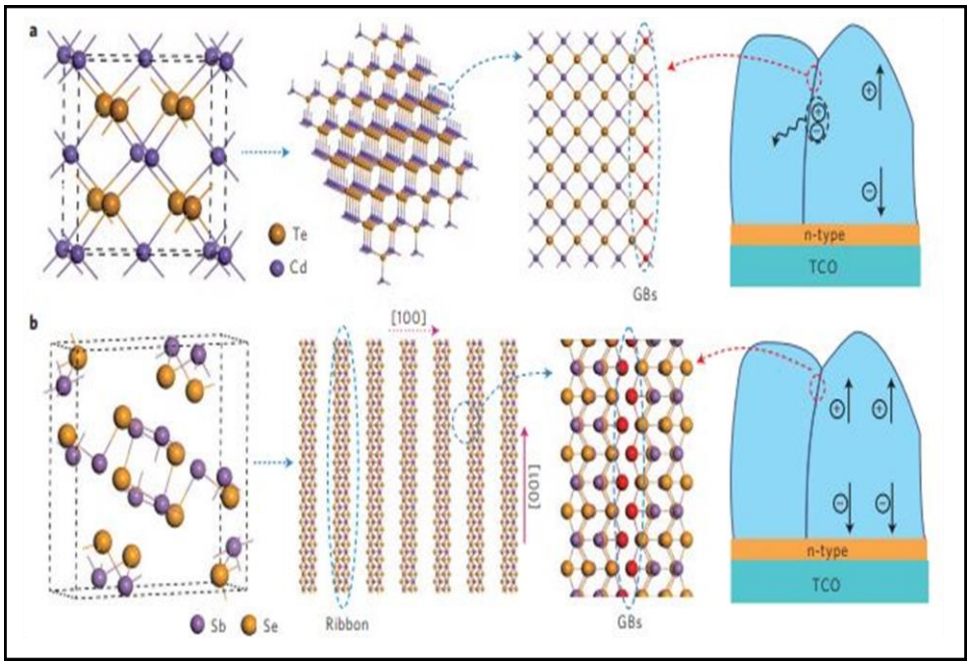

Figure 1. 12 Crystal structure of $Sb_2Se_3$and recombination losses at the GBs in CdTe and Sb_2Se_3

a) CdTe crystal structure and its dangling bonds which result for recombination losses.

b) Sb_2Se_3 crystal structure and mechanism of avoiding recombination losses at GBs.

1.4.2 Sb_2Se_3 journey as an absorber material in thin film solar cells

The first–ever Sb_2Se_3 was used as an absorber layer by Messina, and Nair et al. in 2009, employing deposition method achieved 0.66% photoconversion efficiency[39].

A major breakthrough took place in 2015 as Zhou et al. fabricated CdS/Sb_2Se_3, reporting efficiency of conversion 5.6%[38]. Still, in 2017, Wang et al. were able to achieve photo conversion efficiency(PCE) of 6% with ZnO/Sb_2Se_3 solar cell superstrate configuration[40]. Efficiency improvement was remarkable; in fact, Sb_2Se_3 draw the attention of the researcher's potential material as an absorber layer in the future. More intensively, research works were started by utilizing Closed Space Sublimation (CSS). In 2017, CdS/Sb_2Se_3/PbS superstrate configuration could harvest 6.5% of PCE by Chen et al.[41] Hutter et al. used CSS method to fabricate Sb_2Se_3 in TiO_2/ Sb_2Se_3/PCDTBT superstrate configuration and reported 6.6% of PCE[42]. In the same year, Sb_2Se_3 was deposited using vapor transport deposition (VTD) in CdS/ Sb_2Se_3 to record groundbreaking 7.6% of photo conversion efficiency[26]. So far the highest PCE of 9.2% was achieved in 2019 by Li et al. with substrate ZnO:Al/ZnO/CdS/TiO_2/ Sb_2Se_3/$MoSe_2$/Mo solar cell configuration[43]. Sb_2Se_3 will be better solution for the prevailing toxic absorber layer and the junction engineering in the future.

Past works showed that the solar cell device execution firmly relies upon the direction of the nano ribbons of the absorber layer and, up to this point, a massive piece of researches made on this material has focused on streamlining development conditions to accomplish the ideal direction[44]. For instance, [211] orientations have much better hole mobilities than [020] and [123], which reflects that holes move across the ribbons better than between the ribbons(2.59,1.17, and 0.29 $cm^2V^{-1}s^{-2}$)[45].

1.5 The summary of the literature overview and aim of the study

The project reported in the literature on the CBD CdS thin films and their applications on CdS/Sb_2Se_3solar cells can be summarized as follows:

1. CdS is an ll–V compound and a very prominent and active material in semiconductors. It has properties like wide bandgap, high transparency, tunable n–type electrical properties, the ability to have a wurtzite structure, and the many available fabrication techniques. Because of these properties CdS is used in solar cells as the n–type buffer for many materials like CdTe, CIGS, kesterite absorbers, and Sb_2O_3 in superstrate or substrate configurations.
2. There dry and wet various processes of depositing CdS. RF sputtering and

thermal evaporation are the main dry processes, while CBD is the standard wet process of depositing CdS. CBD has many significant benefits as follows: simplicity, low cost, large–area deposition, conformal coating, controllable thickness, and compatibility with a variety of suitable substrates.

3. As deposited CBD CdS films form in between cubic and hexagonal structure but be inclined towards cubic phase with low crystalline qualities. Thermal annealing can adjust the crystalline attributes by changing the parameters of post–deposition treatments by removing impurities like OH, which is playing a significant role in this study.
4. Improvement of the crystal structure of CdS films has been widely studied using $CdCl_2$ or other halide post deposition treatments. For Sb_2Se_3/CdS solar cell architecture, the $CdCl_2$ treatment of CdS layer at 380-420℃ in air is often applied, however the role and effect of this annealing step for CdS and CdS-Sb_2Se_3 heterojunction interface is not yet understood. Furthermore, there are little systematic investigations on the influence of vacuum and air annealing over the wide range of temperatures on the properties of CBD CdS films and performance of CdS/Sb_2Se_3 device.
5. Systematic studies are required to understand the impact of those annealing procedures on the properties of CBD CdS films and their impact on the formation of Sb_2Se_3/CdS heterojunction interface.

Main aims of this study,

1. To get familiar with the CBD method and to prepare CdS thin films by CBD method.

2. Anneal the sample at different temperatures (200 - 400℃) in vacuum and air.

3. To study the effect of the annealing process on the structural, optical, and electrical properties of CBD CdS films.

4. To depict the physico–chemical processes accountable for the modification in CdS thin film properties consequently of annealing.

5. To apply the annealed CBD CdS thin films in superstrate CdS–Sb_2Se_3 solar cells and study the changes of device properties.

2. CHARACTERIZATION METHODS

2.1 Experimental procedure of CBD CdS thin film deposition

2.1.1 Glass/FTO substrates preparation

Approximately 25mm^2 of glass and soda-lime glasses with coated fluorine–doped tin oxide (FTO) of the thickness range around 150–200nm were immersed in a specific solution. The solution contains 10g–$K_2Cr_2O_7$, 10ml– H_2O, 100ml H_2SO_4 and substrates were immersed 24 hours. Then substrates were cleaned with deionized water left in ultrasonic bath for nearly 5 minutes. Finally, glasses were dried with compressed air.

2.1.2 CBD Deposition and post deposition treatments

CdS thin films were deposited using CBD figure 1.2 apparatus set up on glass substrates and FTO/glass substrates. Approximately 25mm^2 Substrates were appropriately cleaned using the traditional cleaning method, and films were deposited as follows.

Substrates were immersed in a solution of 1 mM $CdSO_4$, 10 mM thiourea, 0.2 M NH_4OH, and 30 mM $(NH_4)_2SO_4$. For CdS doping, a low concentration of NH_4Cl solution (0.1 μM) was added to the deposition bath. The pH, temperature, and agitation speed of the solution were 10.5, 85℃, and 500 rpm, respectively.

After the deposition, substrates were rinsed with deionized water, and all the CdS thin films were annealed in a vacuum at 120℃, and the output samples are called "as–deposited." The reason behind the pre–annealing just after the deposition is to remove most of the secondary phase water, organic impurities, and hydroxides. After that, the main parameter of the study, which is annealing temperature, was carried out in air and vacuum conditions.

Table 2. 1 Annealing temperatures and the time

Condition	Time(min)	Temperature(℃)
Vacuum	30	200,250,300,350,400
Air	30	200,250,300,350,400

2.1.3 Fabrication of Sb_2Se_3 absorber layer

Sb_2Se_3 absorber layer was deposited on to the annealed CdS/FTO/glass by Close Spaced sublimation. In this step, the substrate temperature was 460°C while source was kept at 490°C maintaining the deposition rate of 1µm/min.

2.3Characterization of CBD CdS films

2.3.1 X–ray Diffraction (XRD)

XRD measurements are conducted to determine to study crystal structure, phase composition, and atomic spacing of materials. Non–destructive XRD measurements are being carried out for thick materials or powder–like materials as X–rays have penetration ability. X–rays are produced in a cathode ray tube by heating a filament. These electrons are accelerated by applying a voltage to bombard towards target materials. When bombard electrons have adequate energy to extricate inner shell electrons, characteristic X–ray spectra are created. Copper (Cu) is the most common target material for single–crystal diffraction, with Cu K_α radiation=1.5418Å. The sample with the detector is being rotated while these X–rays are collimated and directed onto the sample[46]. Bragg's equation describes the diffraction of X–rays Hence, Brigg's Law can be expressed as follows [47].

$$2d \sin\theta = m\lambda \text{v} \qquad 2.1$$

Where,
d – Inter–planer distance
θ – Angle between the incident X–ray beam and the two parallel atomic planes
m – Order of diffraction
λ – Wavelength of the incident X–ray beam
Annealing temperatures and the time
X–rays with constant wavelength are directed towards target material, X–rays diffracts from crystal atoms illustrated figure 2.1 , which is captured by detector[48],

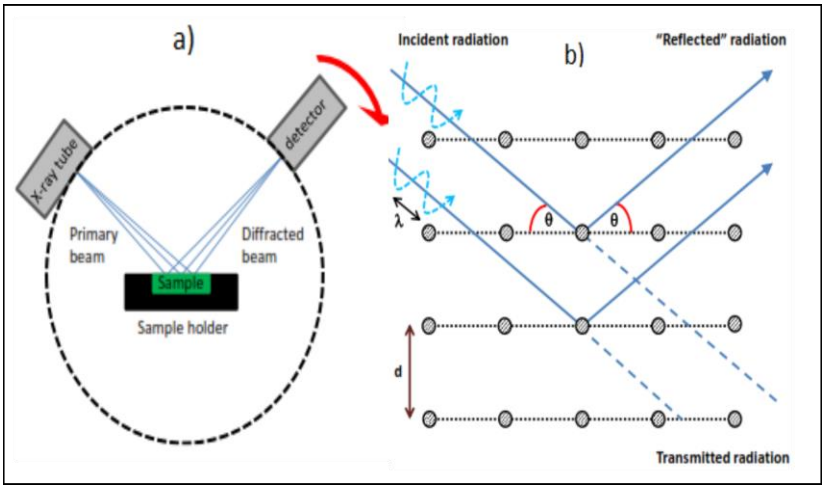

Figure 2. 1 Scheme of XRD measurement and b) Bragg's geometry of X–rays reflection

From the XRD patterns, the crystallite size (L) was obtained by the Scherrer equation (2.2), where B is the peak width, *K* is the Scherrer constant, lambda is the wavelength of X–radiation, and *θ* is ½ the diffraction angle.

$$\mathbf{B(2\theta)} = \frac{\mathbf{K\lambda}}{\mathbf{L cos\theta}} \qquad 2.\ 2$$

In this project, Siemens D5000 diffractometer was used, with emission at the Cu Kα radiation=1.5418Å. Operations were conducted in the range of 2θ=200–800 with an X–ray tube setting of 40kV and 40mA for all samples.

2.3.2 Scanning electron microscopy

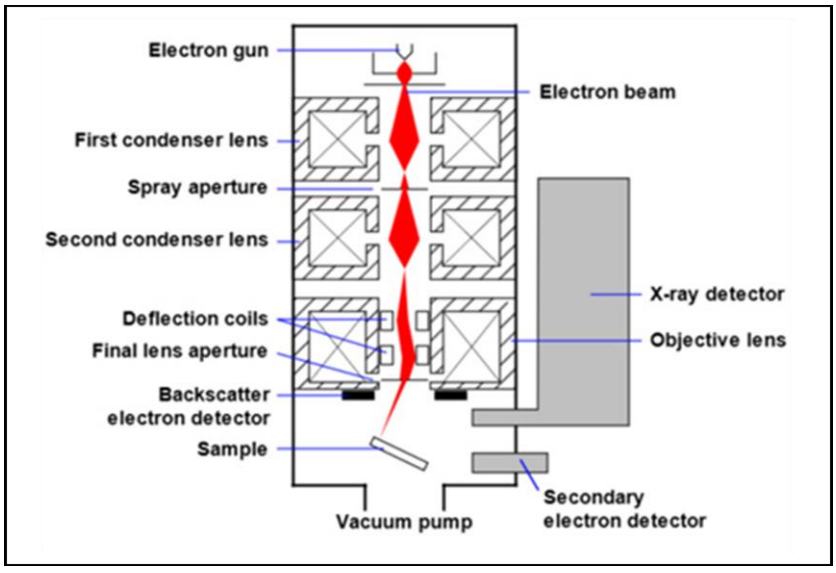

Figure 2. 2 Cross section of SEM from sample to detector

SEM figure2.2[25] is an excellent characterization method using secondary electron emission when they bombarded to target materials to insight thin film's morphology, grain size, and thickness. SEM can be used in other forms of characterization like energy dispersive X–ray analysis and electron beam induced current.

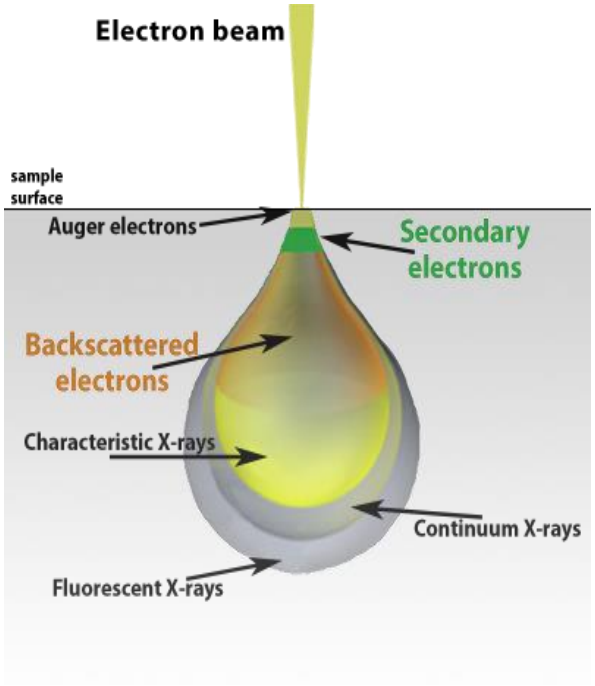

Figure 2. 3 Schematic of the SEM electron beam through the sample

Electrons are delivered at the highest point of the column, quickened down, and went through a mix of lenses and gaps to create an engaged beam of electrons that hits the outside of the sample. The sample is mounted on a phase in the chamber zone, and, except if the microscope is intended to work at low vacuums, both the column and the chamber are emptied by a mix of pumps.

The (SEM) produces images by scanning the sample with a high–energy beam of electrons. As the electrons interact with the sample, they have secondary electrons, backscattered electrons, and characteristic X–rays. These signals are gathered by at least one detector to frame images shown on the computer screen. When the electron pillar hits the outside of the sample, it infiltrates the sample to a profundity of a couple of microns, contingent upon the accelerating voltage and the thickness of the sample. Numerous signals, similar to secondary electrons and X–rays, are delivered because of this association inside the sample[49].

2.3.3 Van der Pau method

Vand der Pau (VDP) is a four–probe method that is widely used to determine the sheet resistance of thin films. In the apparatus setup, 4 points were chosen in the corners of a square, as shown in figure 2.4.

We are considering homogeneous electric conducting thin film with uniform thickness with four contacts.

In the first experiment, a current I_1 is supplied through contacts A and B, and the voltage drop V_1 across the remaining contacts C and D is measured, as shown in figure 2.4(a). In the second experiment, a current I_2 is fed through A and D, and the voltage drop V_2 is now measured across the contacts B and C figure 2.4(b)[50]. Using conformal mapping techniques, VDP proved that the following relation holds[50].

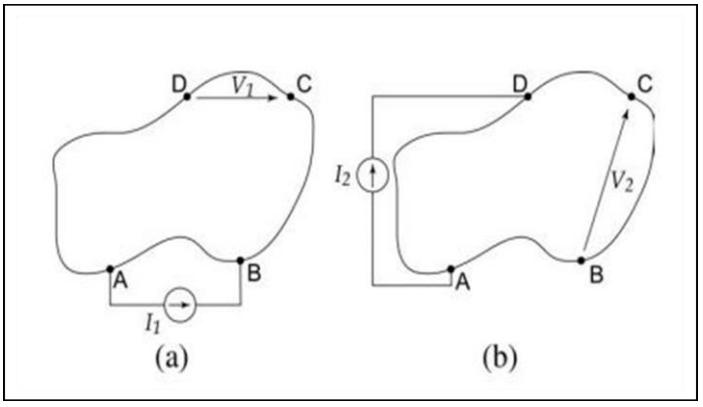

Figure 2. 4 Four probe method

The relation can be given as equation 2.3[50],

$$\exp\left(-\pi\frac{V_1}{I_1 R_S}\right)+\exp\left(-\pi\frac{V_2}{I_2 R_S}\right)=1 \qquad 2.\ 3$$

Where R_s is the sheet resistance.

2.3.4 Hall Effect

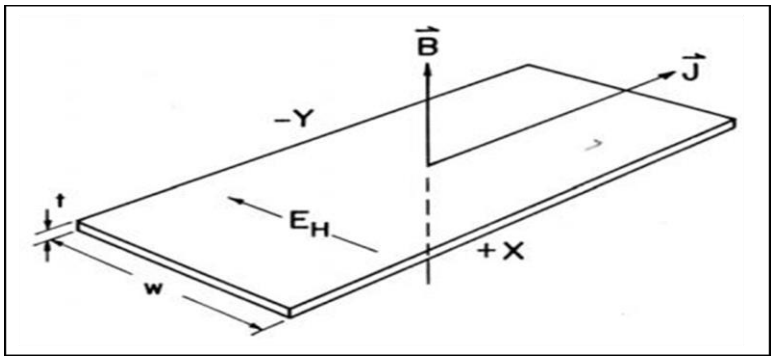

Figure 2. 5 Schematic diagram of Hall Effect.

Hall Effect can be performed on the VDP configuration to find electrical properties such as resistivity, carrier concentration, and hall mobility. When the current–carrying thin film is placed in a slanting magnetic field, the Lorentz force on the moving charges produces a voltage perpendicular to both the field and the current known as Hall Effect[51] figure 2.5[51].

When the supply current I and magnetic field is B, hall coefficient R_H is given as in equation 2.4[51],

$$\mathbf{R_H = \frac{E}{JB} = \frac{tV_H}{IB} = \frac{1}{ne}} \qquad 2.\ 4$$

V_H is the hall voltage, n is the density of charge carries, e is the charge of an electron, and t is the thickness of the thin film.

The drift velocity (v_d) can be given as[51],

$$\mathbf{J = \frac{I}{A} = nev_d} \qquad 2.\ 5$$

Where A is the cross–sectional area of the thin film. The mobility is defined as follows[51],

$$\mathbf{\mu = \frac{v_d}{E} = \frac{1}{\rho ne}} \qquad 2.\ 6$$

2.3.5 UV–vis spectroscopy

When the thin–film materials are irradiated to EM waves, absorption, transmission, reflection, and scattering occur. This wave–like nature of EM waves is commonly used for optical characterization to find absorption coefficient and bandgap energy.

When CDS thin films are exposed to the photons having the required energy for

possible electronic transfers, some of the light will be absorbed by the materials as the energy required for electron transition from the valance band to the conduction band. At the same time, the rest will be transmitted, reflected, or scattered. The optical spectrum is recorded as a graph of absorbance vs. wavelength or reflectance vs. wavelength.

The absorption coefficient can be calculated using equation2.7[52],

$$\frac{\mathbf{T}}{\mathbf{100-R}} = \mathbf{e}^{-\alpha \mathbf{d}} \qquad 2.7$$

Where T is the transmittance, R is the reflection, α is the absorption coefficient and d is the film thickness.

The optical band gap can be calculated from the Tauc's equation2.8[52],

$$(\boldsymbol{\alpha h\nu})^{\mathbf{n}} = \mathbf{A}\left(\mathbf{h\nu} - \mathbf{E_g}\right) \qquad 2.8$$

Where A is a constant, his Planck's constant, α is the derived absorption coefficient from equation 2.8,v is light frequency. N can be 2 for direct bandgap materials while 0.5 for indirect bandgap materials.

From the graph of$(\alpha h\nu)^2$ vs. hν, E_g can be derived by extrapolating the linear part.

2.4 Characterization of solar cells

2.4.1 Current–voltage characterization of solar cells

Solar cell demonstrates the characteristic behavior of the diodes under the illumination. I–V measurement is one of the measurements that we can conclude about the quality of the solar cells. To characterize CdS/Sb_2Se_3 solar cells,

According to figure 2.6[53], the dark line represents the I–V curve in the dark, while the yellow line represents the I–V curve when solar cells are illuminated to the light. In the dark, there is no photocurrent, while in the illuminated states, photocurrent is generated.

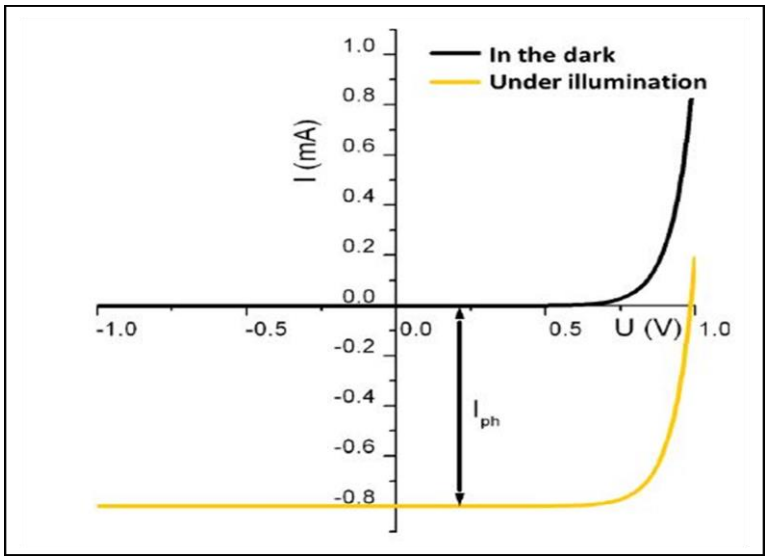

Figure 2. 6 Solar cell J–V curves in the dark (Black) illuminated (Yellow)

According to the Schockley diode equation, which represent the solar cell states in the dark equation 2.9[54],

$$\mathbf{J = J_0\left(e^{\frac{qV}{AkT}} - 1\right)} \qquad 2.\ 9$$

J is the current density, J_0 is the saturation current density, V is the applied voltage, q is the charge of an electron, A is the diode ideality factor, k is the Boltzmann's constant, and T is temperature.

When illuminated to the light, photocurrent density (J_{ph}) is added to the equation 2.10[55],

$$\mathbf{J = J_0\left(e^{\frac{qV}{AkT}} - 1\right) - J_{ph}} \qquad 2.\ 10$$

From the I–V curve, standard device performance parameters like short circuit current density (J_{SC}), where the load on the solar cell is zero–rated, and the voltage at the contacts is zero, open–circuit voltage (V_{OC}) where the point represents no load is applied to the contacts of the solar cell, and the current through the solar cell is zero, fill factor (FF) and efficiency can be measured. The efficiency of the solar cell is more significant when the J_{SC}, V_{OC} are higher [69].

Both V_{OC} and J_{SC} can be determined from the I–V curve. V_{OC} is when the curve intersects the x–axis, and J_{SC} is the point where the curve crosses the y–axis figure 2.7[53].

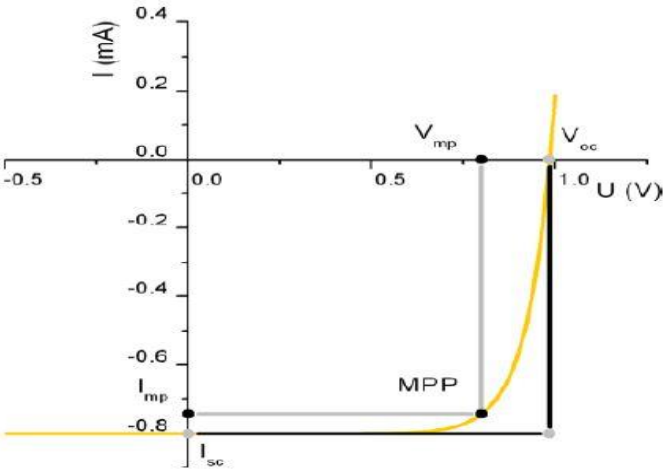

Figure 2. 7 Solar cell J–V curve illuminated state. MPP is the maximum power mode solar cell is operating

The fill factor is the power loss of a real solar cell. FF as shown in the equation 2.11[56] is the ratio between MPP (maximum power point) and the V_{OC}*J_{OC}. MPP can be determined from the I–V curve, as shown in figure 2.7.

$$FF = \frac{P_{mp}}{J_{SC}V_{OC}} = \frac{J_{mp}V_{mp}}{J_{SC}V_{OC}} \qquad 2.\ 11$$

Efficiency is the ratio of the maximum output power generated by the solar cell to the incident light power (P_s) equation 2.12[57]

$$\eta = \frac{V_{mp}J_{mp}}{P_s} \qquad 2.\ 12$$

2.4.2 External Quantum Efficiency (EQE)

The simple definition of quantum efficiency is as follows[58],

$$Quantum\ Efficiency = \frac{The\ number\ of\ carriers\ collected\ by\ the\ solar\ cell}{The\ number\ of\ photon\ of\ a\ given\ energy\ incident\ on\ the\ solar\ cells} \qquad 2.13$$

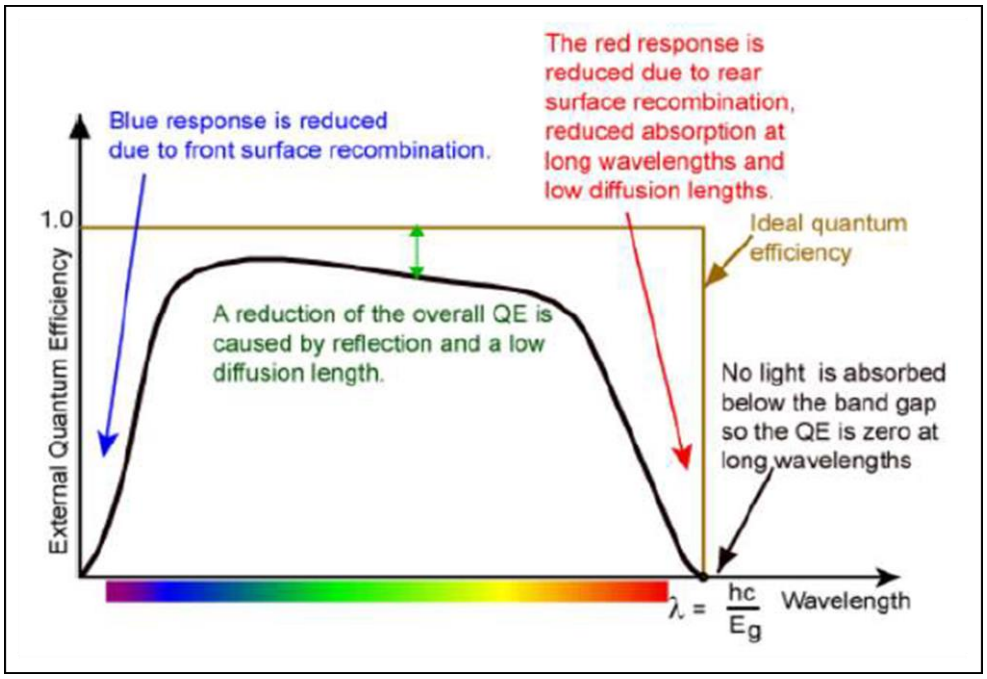

Figure 2. 8 Quantum efficiency of a non–ideal solar cell and an ideal solar cell

EQE is given as a function of wavelength or as a function of energy. Mainly there are two types of quantum efficiencies as external and internal. By measuring the reflection and transmission of a solar cell device, both external and internal quantum efficiency curves can be obtained Ideal solar cell represent in a square shape behavior while practical solar cells deviate from this behavior due to absorption coefficient, charge separation/collection and recombination effects[58].

3. RESULTS AND DISCUSSION

3.1 Influence of the thermal annealing on the CBD CdS buffer layer properties

This section is focused on investigation of changes in structural and optoelectronic properties of CBD-CdS single layers deposited on glass substrates, modified by vacuum and air annealing at various temperatures. The mechanism of physicochemical processes responsible for the changes in the properties of the CdS films are proposed.

3.1.1 Electrical properties

Electrical resistivity and carrier concentration of the CdS films, which were annealed in air and in vacuum at different temperatures, were measured using the Van der Pauw method and Hall measurements at room temperature. First, it is important to note that Hall measurements showed strong n-type conductivity for CdS films. As seen in Fig. 3.1, the electron concentration of CdS films is dependent upon the temperatures at which air and vacuum annealing were carried out. Given the electron concentration of as-deposited CdS film was 10^{15} cm^{-3}, both types of annealing at temperatures 200–300°C clearly increased electron concentration.

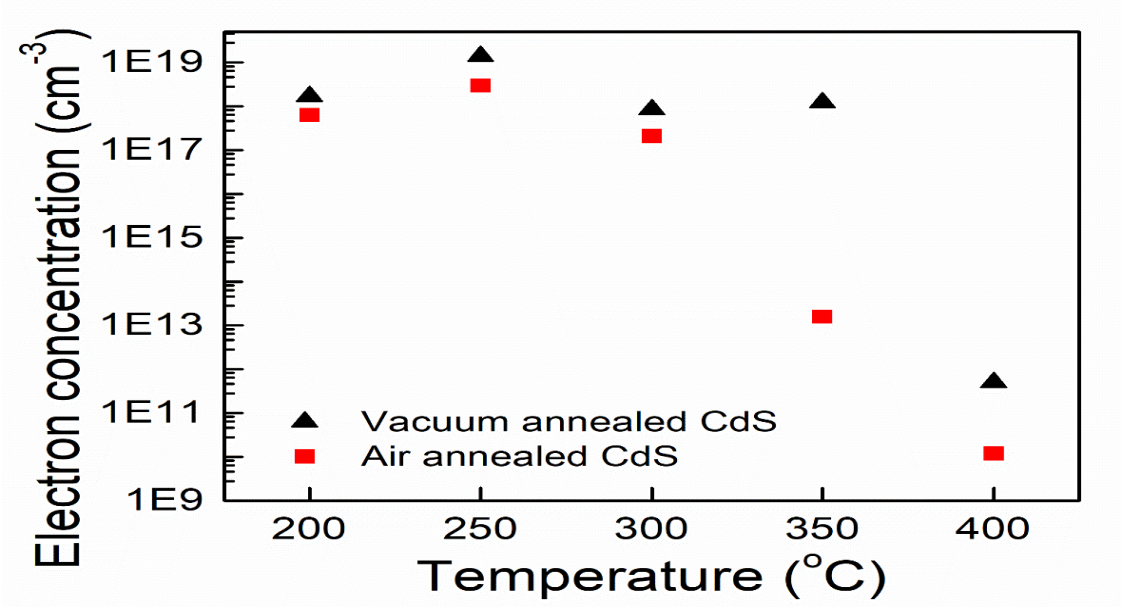

Figure 3. 1 Graphical representation of electron density vs annealing temperature of CBD CdS in air and vacuum at 200-400°C

Maximum electron density was achieved at 250°C in both air and vacuum annealing, showing 10^{18} cm^{-3} and 10^{19} cm^{-3}, respectively. It can be noted that from 350°C onwards, there is a clear decline in the electron concentration.

Table3.1 shows the resistivity, mobility, and electron concentration of the CdS films. Compared with as-deposited CdS films, resistivity is significantly reduced at annealing temperatures 200 and 250°C. These results obtained from van der Pauw measurements correlate well to the Hall results presented above. Similarly, resistivity shows substantial increase at temperatures 300–400°C from 44.8 Ω·cm to 42570.0 Ω·cm in air and from 8.5 Ω·cm to 10298.0 Ω·cm in vacuum.

Behavior after 350℃ is strange as the resistivity increased and the mobility has been increased. The reason for this may be due to the growth of interactions in the lattice of crystallites at the atomic level restricted by the diffusion process or as a result of sample inhomogeneity[59]. CdS mobility shows the intrinsic behavior of the materials like other materials like CdSe, ZnO, and ZnS[59]. Another reason for this behavior of carrier concentration, resistivity at higher annealing temperatures (>300°C) due to contamination of the films by alkali ions from glass substrates[60]or by a change in the Cd/S or other ions ratios. At lower temperatures CdS shows the intrinsic behavior from decreasing resistivity.

Table 3. 1 Electrical properties comparison with the annealing temperature

T(^{0}C)	Resistivity(Ωcm)		Mobility(cm^2/Vs)		Density(cm^{-3})	
	Air	Vacuum	Air	Vacuum	Air	Vacuum
As dep	284.0	284.0	5.0	5.0	–4.4E+15	–4.4E+15
200	4.2	3.2	3.1	1.2	–6.3E+17	–1.7E+18
250	2.6	0.2	3.3	2.2	–3.0E+18	–1.4E+19
300	44.8	8.5	0.7	0.9	–2.1E+17	–8.5E+17
350	7717.3	45.8	61.1	1.0	–1.6E+13	–1.2E+18
400	42570.0	10298.0	12460.0	1360.8	–1.2E+10	–5.0E+11

3.1.2 Structural properties

Figure 3.2 (a and b) shows the X–ray diffraction patterns of CBD CdS films annealed in air and vacuum at 200–400℃.

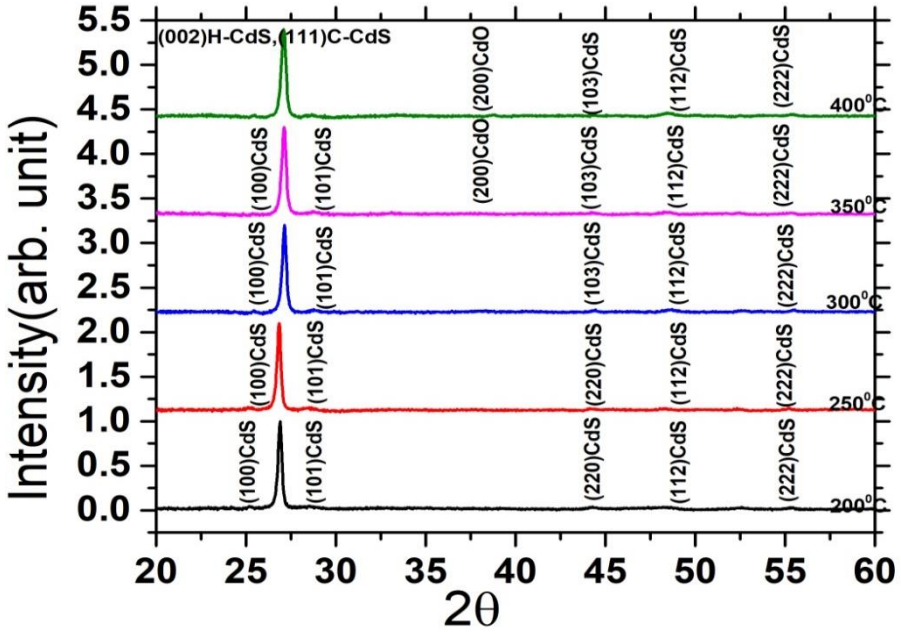

Figure 3. 2 (a) XRD patterns of CBD CdS films annealed in air at 200-400°C for 30min

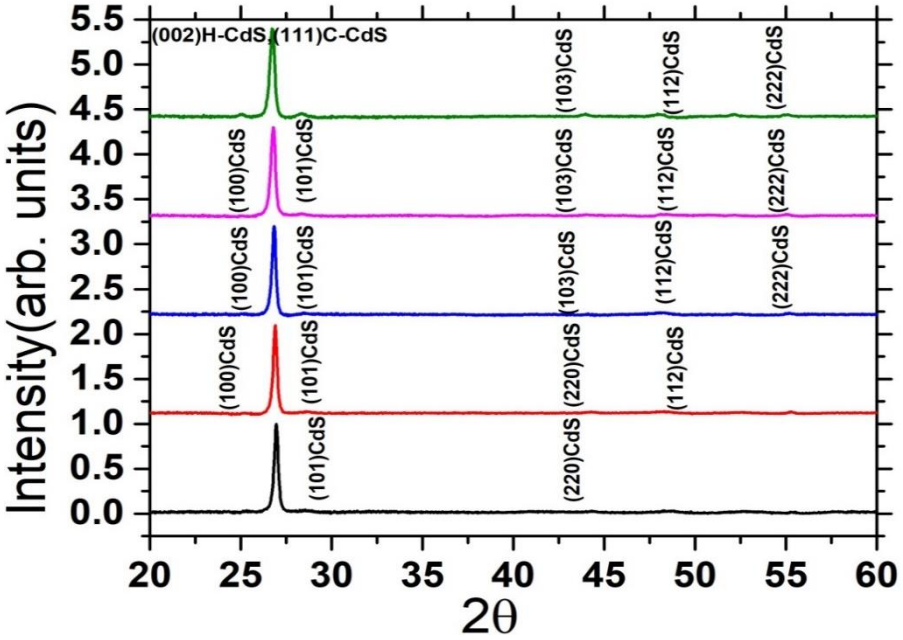

Figure 3. 2 (b) XRD patterns of CBD CdS films annealed in vacuum at 200-400°C for 30 min

The diffractograms show a similar pattern for both, air and vacuum annealing conditions with a single predominant peak in the range from 26.4–27.0 ^{0}[55], [61]. This peak is attributed to either (002) plane from hexagonal structural orientation or (111) plane of cubic orientation. Both air and vacuum annealed CdS films demonstrate strong peak at 26.7^0 and hardly visible peaks at 44.3^0, and 52.3^0, which are linked CdS with the (002),(103), and (112) of the hexagonal crystal structure (ICDD: 01–089–0440) or (111), (220), and (331) of the cubic modification[62].

Peaks matching to indications from (002), (103), and (112) of hexagonal CdS are present in all annealed samples. Both patterns Fig. 3.2 (a) and (b) show amplified XRD peak intensity and sharpening the main peak when increasing the annealing temperature from 200°C to 300°C, while after 300°C intensity of the peak is going down. The slight shift of hexagonal CdS peak (002)–26.8^0 to the cubic (111)–26.4^0[6] CdS direction can be observed in both, vacuum and air annealing conditions. However, the trend in the displacement of the XRD peak towards cubic phase Fig. 3.3 was more pronounced for the vacuum annealing. In contrast, for the air treatment procedure, the same peak initially shifted towards lower 2theta values (to cubic modification), as a result of treatment at 250°C, while for 300°C air annealing, a prominent displacement of the peak towards higher 2θ values was observed. At 350°C and 400°C air treatment the peak shift followed the same trend as for lower annealing temperature but with a very small step.

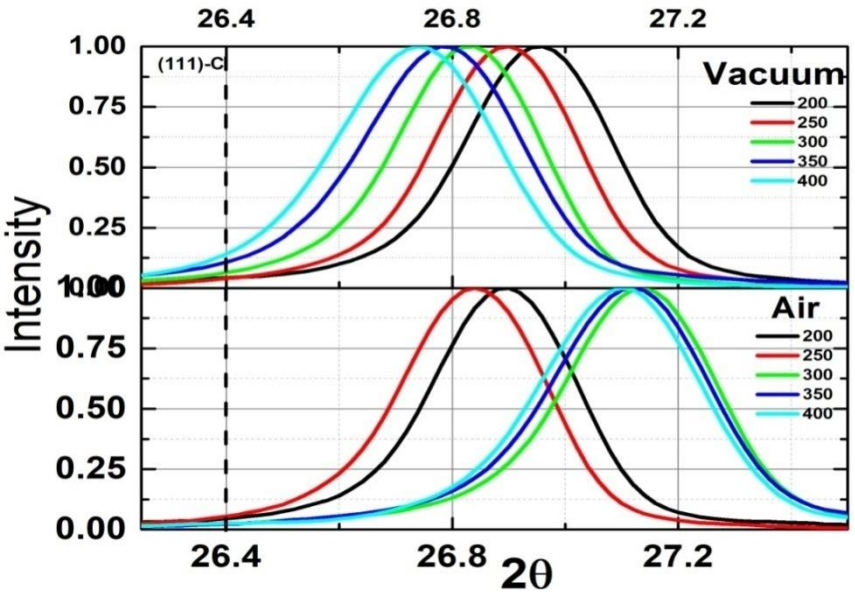

Figure 3. 3 Displacement of the (111) peak with increasing of temperature of CdS annealed in air and vacuum at 200-400°C

Figure 3.4 illustrates the behavior of interplanar distance and the lattice constant with the temperature. The values of interplanar distance together with crystallite size and lattice parameter are summarized in Table 3.2. The lattice constant and interplanar distances increase with the increase of the annealing temperature.

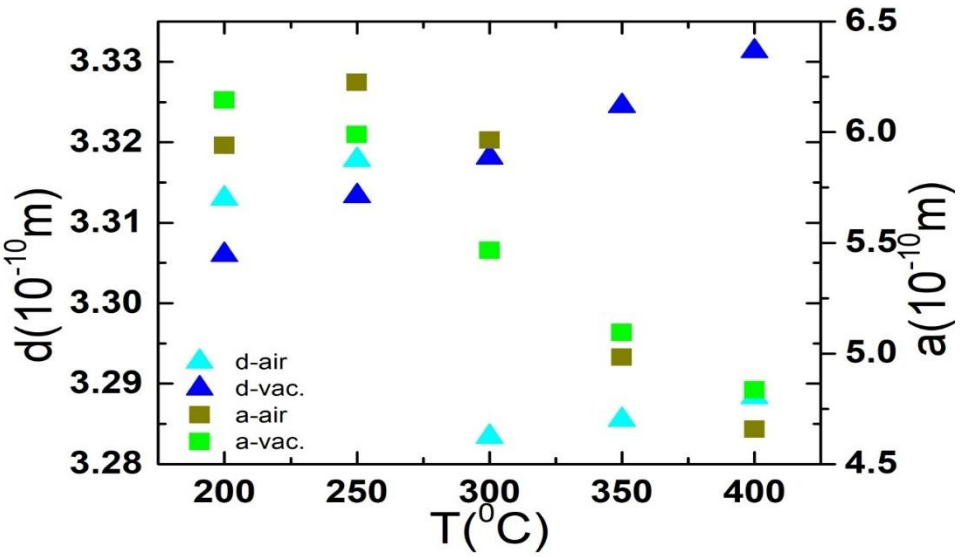

Figure 3. 4 Variation of interplanar distance (d) and lattice constant (a) of CBD CdS with annealing temperature

Table 3. 2 Crystallite size(S), interplanar distance (d) and lattice constant (a) for CBD CdS annealed at different temperatures.

Temperature	S(nm)		d(Å)		Lattice Constants(Å)	
					Air	Vacuum
	Air	Vacuum	Air	Vacuum	a	a
200	61.4	59.4	3.313	3.306	5.74	5.73
250	59.9	62.3	3.318	3.313	5.75	5.74
300	54.6	59.6	3.283	3.318	5.69	5.75
350	50.9	49.8	3.286	3.325	5.69	5.76
400	48.3	46.6	3.288	3.331	5.70	5.77

According to the main peak shift figure 3.3, from hexagonal configuration to cubic structure, we can hypothesis as deposited CBD CdS has mainly cadmium hydroxide complex $CdS_{1-n}(OH)_n$ as $Cd(OH)_2$ physically crystallizes into a hexagonal lattice while CdS and CdO be likely to grow in cubic structures. The main peak shift in a vacuum

has a comprehensible structure transformation, whereas, in air, it shows a wobbly main peak shift but generally transforms from hexagonal to the cubic structure.
Thermally annealed in air and vacuum connected with the interaction between CdS, O_2 and $CdCl_2$ proposed in McCandless studies [78].

$$2NH_4Cl + CdSO_4 \rightarrow CdCl_2 + (NH_4)_2SO_4 \quad 3.1$$

CdS are highly soluble in $CdCl_2$ while oxygen diffuses into the melted phases promoting formation of CdO and $CdSO_3$
Extracted in the air as shown as following,

$$CdS + CdCl_2 + O_2 \rightarrow SCl_2 + 2CdO \quad 3.2$$

$$CdS + 1.5O_2 \rightarrow CdO + SO_2 \quad 3.3$$

$$\mathrm{CdS} + 1.5\,O_2 \rightarrow \mathrm{CdSO_3} \quad 3.4$$

Annealing temperatures above 350^0C, $CdSO_3$ further decomposes into CdO.

$$\mathrm{CdSO_3} \rightarrow CdO + SO_2 \quad 3.5$$

In vacuum, oxygen cannot diffuse into the melted phases and only decompose of $Cd(OH)_2$ complex into CdO, resulting in a proper shift peak to the cubic phase.
According to the previous studies on CBD CdS[19], the minor peaks emerge in the air after heat treatment at 400°C due to the reflection from (200) CdO and (033) $CdSO_3$. The appearance of the CdO phase might be due to the oxidation of hexagonal CdS. According to the structural analysis of CBD CdS, we can rarely able to identify creating of the CdO phase in the air while in a vacuum; we could not find any CdO phase. The basic ammonium medium controls highly conductive CdO formation was used in the chemical bath.

Figure 3.5 display the surface and the cross–sectional SEM images of CBD CdS/glass structures after annealing in air and vacuum. The surface of as–deposited CBD CdS featured with bulky accumulated particle clusters, and CBD CdS grains grow perpendicular to the substrate with a columnar shape maintaining small grains figure 3.5(a). As the temperature increases, particles possess an evenly spaced surface with the help of recrystallization during the annealing process.
The porosity of CdS responsible for intra–grain recrystallization and sintering of the primary grains as shown in Figure 3.5 (a). The morphology of CBD CdS drastically changes with the annealing temperature. In both air and vacuum, the oxidizing ambient enhanced the grain growth up to 250°C after that ambient contracted the grains at a rapid rate significantly figure 3.5(d) (e). From the surface morphology, we can conclude with previous studies; maximum temperature for thermal annealing

CdS is 400°C while up to 250°C demonstrates optimal grain structure. Apart from that, at 400°C, it creates pinholes in the CdS film Fig 3.5 (e).

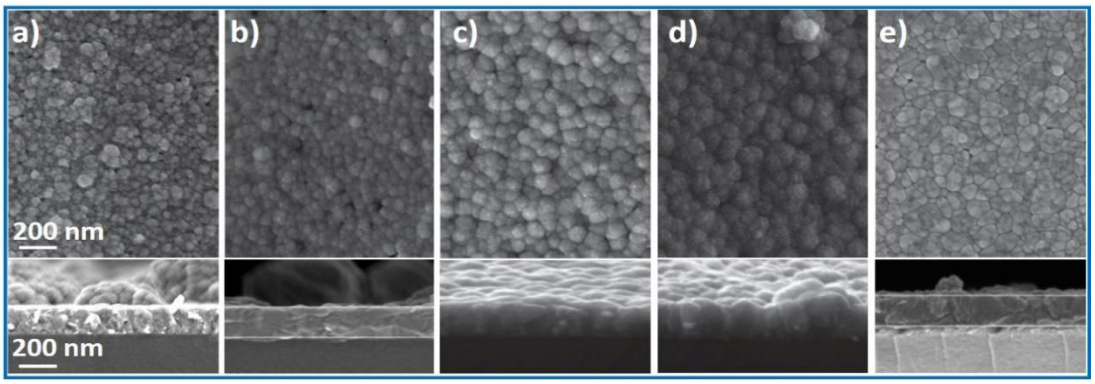

Figure 3. 5 The surface of and the cross section of CBD CdS on glass a) As deposited b) Annealed in vacuum at 200°C c) Annealed in air at 200°C d) annealed in vacuum at 400°C e) Annealed in air at 400°C

The surface morphology and cross section of CBD CdS/FTO is shown as follows figure 3.6. Based on SEM of CBD CdS/FTO and CBD CdS/glass, we observed that as–deposited films are not dense. It is easy to have dense films at higher temperatures. However, the films demonstrate rough, inhomogeneous surfaces with overgrowth grains.

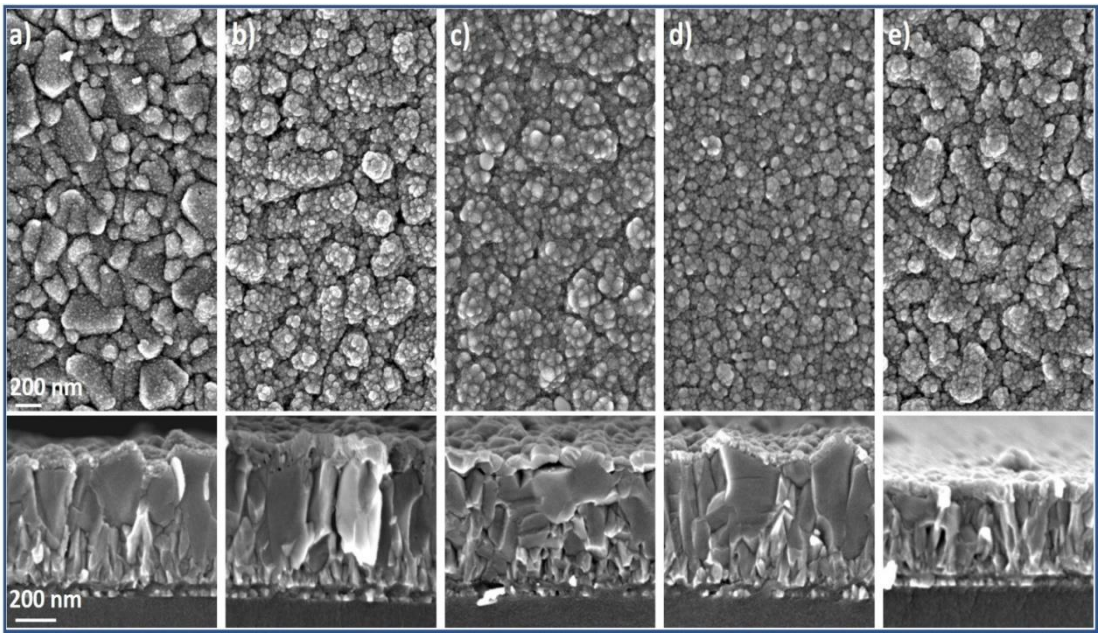

Figure 3. 6 The surface of and the cross section of CBD CdS/FTO a). As deposited b) Annealed in vacuum at 200°C) Annealed in air at 200°C d) annealed in vacuum at 400°C) Annealed in air at 400°C

3.1.3 Optical characterization

The CBD CdS films in air and vacuum show high transmission (65–85%) in the visible range. Extrapolating the curves of transmission vs wavelength in air and vacuum, it was found the bandgap of CdS films varied from 2.3–2.4eV as presented in figure 3.7. As the temperature increases, the bandgap energy (E_g) shifter towards the green wavelength region reflects improvement in crystallinity.

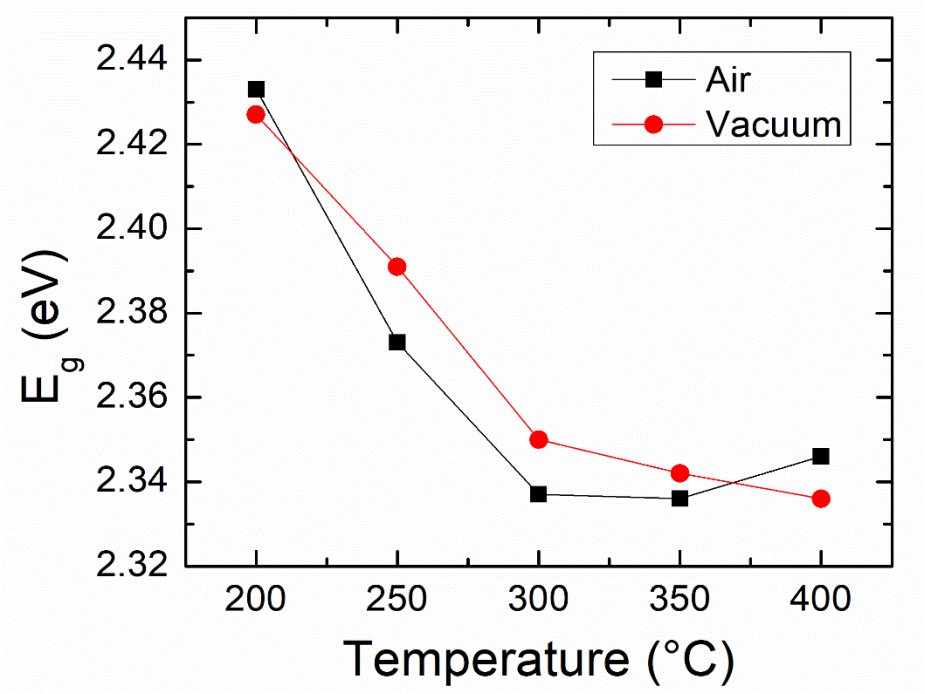

Figure 3. 7 Band gap of CBD CdS thin films annealed in air and vacuum at 200-400°C

Changes in the structural and optoelectronic properties of annealed CBD CdS films can be described with the help of the previous studies. The behavior of thermally annealed CBD CdS thin films can be described in two stages using a physic–chemical mechanism.[19][24]

Considering the growth mechanism of CBD CdS and previous studies, it can predict that the [OH^-] group may act as the shallow donor instead of the sulfur site, thus arising the cadmium complex (cadmium hydroxysulfide) later on CdS is formed by dissolving this complex slowly to gain Cd^{2+} and S^{2-}.[6], [63]

$$nCdS + Cd(OH)_2 \rightarrow Cd_{n+1}Sn[2(OH)_sV_{cd} \quad 3.6$$

Needed sulfide anion comes from the thiourea hydrolysis as follows,

$$SC(NH_2)_2 + OH^- \rightarrow HS^- + H_2O + CN_2H_2 \quad 3.7$$

$$HS^- + OH^- \leftrightarrow S^{2-} + H_2O \quad 3.8$$

According to equations 3.7 and 3.8, hydroxide anion acts as a catalyst for thiourea decomposition, and CdS formation takes place on the surface of hydroxide.

The solution medium should be alkaline to break down thiourea and to get S^{2-}. Adding ammonium to the bath will help to maintain the higher pH level, and it decides the concentration of free Cd^{+2} ions but, it also helps to form a complex with ammonium as follows.

$$Cd(OH)_2 \leftrightarrow Cd^{2+} + 2OH^- \quad 3.9$$

$$[Cd(NH_3)_4]^{2+} \leftrightarrow Cd^{2+} + 4NH_3 \quad 3.10$$

$$NH_3OH \leftrightarrow 4NH_3 + OH^- \quad 3.11$$

Stage 1: T ≤ 250°C

When CBD CdS thin films are thermally annealed, the cadmium complex becomes unstable and decomposes due to the excessive energy supplied thermally. This converts cadmium hydroxysulfide into cadmium oxysulfide creating sulfur vacancies and releasing water as follows,

$$Cd_{n+1}Sn[2(OH)_sV_{Cd}] \xrightarrow{\leq 250^0C} Cd_{n+1}Sn[2O_sV_sV_{Cd}] \quad 3.12$$

When the annealing process started, sulfur vacancies [V_s^{+2}] have been increased, which implies that the reduction of cadmium vacancies [V_{Cd}^{2-}].

Stage 2: T > 250°C

The behavior of temperatures above 250°C is out of the ordinary. But, defending our hypothesis; this can be explained as follows. During the annealing process, $Cd(OH)_2$ converts to CdO, which implies that the product is also enriched with cadmium[19]. Impurities like $(OH)_s^+$ and Cl_s^+ start to behave as shallow donors as a result of this excessive amount of Cd. This is the main reason for increasing electron density at lower temperatures <250°C. Even though, at higher temperatures, decomposing the cadmium complex is accelerated, the electron density starts to drop heavily by 4– 5 times as a result of removing shallow donors.

Another reason for this may be the structural transformation from hexagonal to cubic discussed in the section 3.1.2. The conductivity in air and vacuum has been increased until the temperature 250°C. Another reason can be crystalline size increases considerably with the increase in annealing temperature, thus reducing the grain boundary scattering and increasing conductivity.

According to the argument, "$Cd(OH)_2$ diffuse into CdS lattice during the deposition process" has a robust establishment from E_g's behavior in both air and vacuum. As deposited CBD, CdS has higher band gap values (2.42eV), and this is associated with

the higher bandgap value of $Cd(OH)_2$. When the annealing process is accelerated, the destruction of the incorporated hydroxide group is accelerated. Thus, the thermal process helps to sinter deposited polycrystalline CdS and destruction of hydroxide group resulting in CdO and water.

3.2 Impact of CBD CdS annealing conditions on the properties of CdS/Sb_2Se_3 solar cells.

3.2.1 Effect of CBD CdS annealing on structural properties of Sb_2Se_3 absorber layer.

Upon the post–deposition treatment of CdS films deposited on glass/FTO substrates, Sb_2Se_3 absorber layers were deposited onto CdS films. Solar cells were completed by the deposition of Au back contact. XRD measurements showed orthorhombic crystal structure for the Sb_2Se_3 absorber layer.

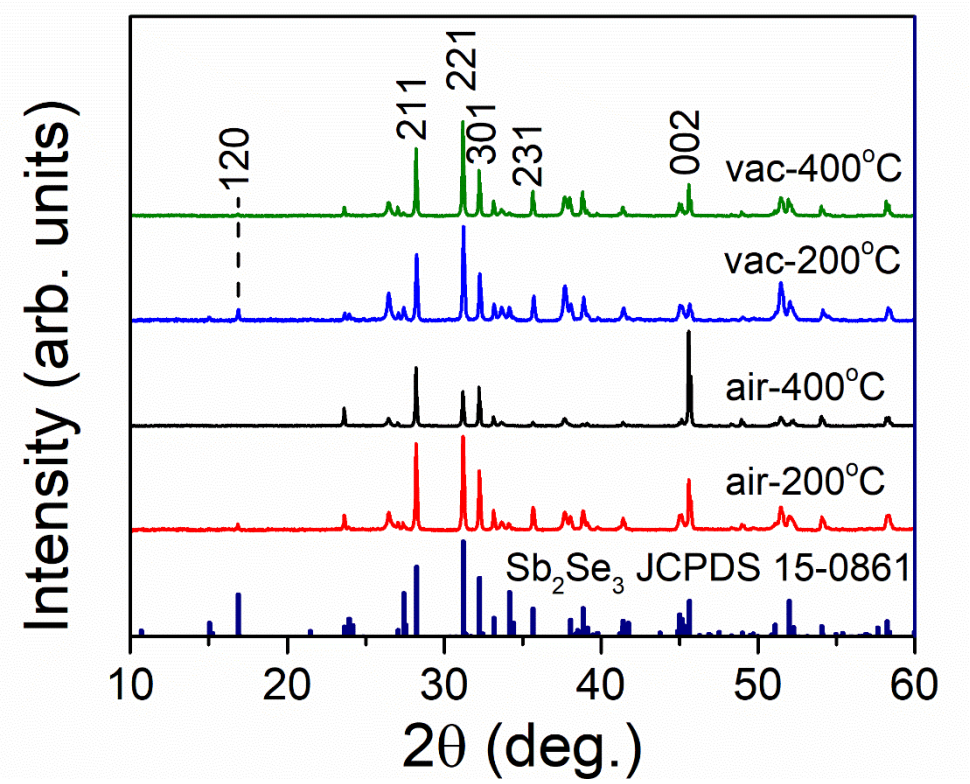

Figure 3. 8 XRD patterns of air and vacuum annealed CBD CdS in air (at 200°C and 400°C) and in vacuum (at 200°C and 400°C) of CdS/ Sb_2Se_3solarcell devices

Figure 3.8 demonstrates the XRD patterns of glass/FTO/Sb_2Se_3/CdS solar cell

devices. Sb_2Se_3 absorber layer was deposited by close–spaced– sublimation method (CSS) at substrate temperature 450°C and source temperature was 520°C. Sb_2Se_3 diffraction peaks were analyzed according to PDF JCPDS 07–089–0821 and PDF JCPDS 15–0861. In both conditions, peaks at 28.2^0, 31.1^0, 32.2^0, 45.1^0, and 45.6^0 are prominently present in all solar cell devices, which respectively belong to (211), (221), (301), (151), and (002) crystal planes. These peaks represent the orthorhombic Sb_2Se_3 crystal orientation.

The surface of and the cross–section of the CdS/Sb_2Se_3 solar cell is presented in Figure 3.9. The optimal CBD CdS annealing temperature to facilitate the fabrication of Sb_2Se_3 with columnar sintered grains is 200°C. Device annealed in the air created highly textured columnar CBD CdS through the recrystallization and sintering due to presence of oxygen–containing phases. For better performance of a solar cell, we expect to have high–quality Sb_2Se_3 with an optimal thickness, minor surface roughness, and large grains are required. From the top view and the cross–sectional view, the film's roughness fabricated using CBD CdS annealed in air has decreased compared to the as deposited films. Moreover, the thickness plays a significant role as the thickness has increased compared to the as–deposited and it reflects a better absorption in the more extended wave length region.

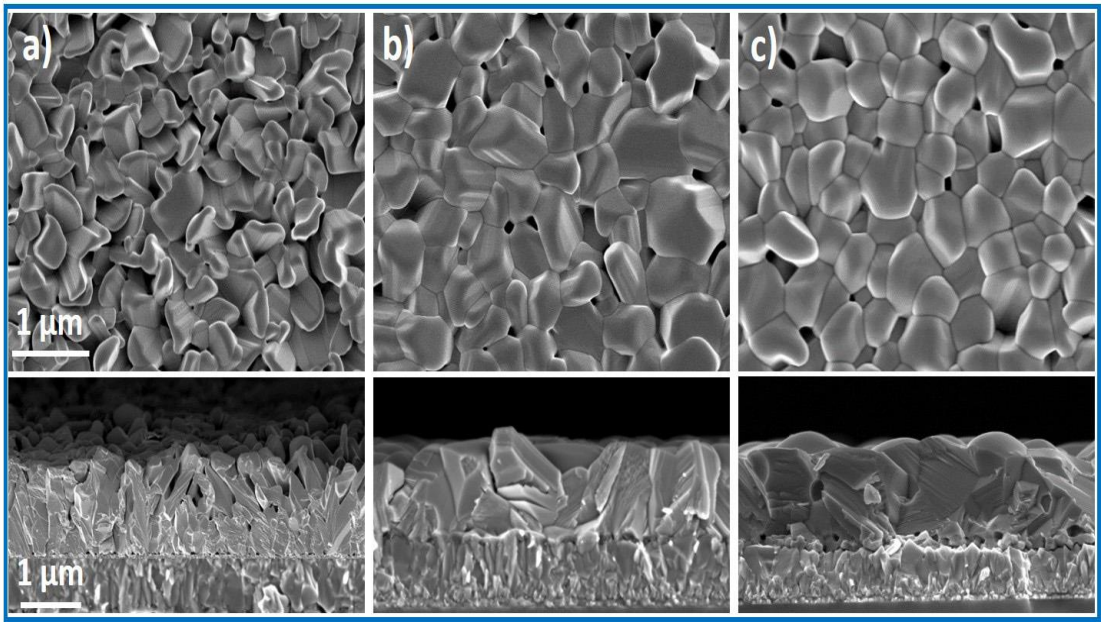

Figure 3. 9 The surface of and the cross section of CdS/ Sb_2Se_3solarcell device a) As deposited of CdS b) Annealed CBD CdS in vacuum at 200°C) Annealed CBD CdS in air at 200°C

3.2.2 CdS/Sb_2Se_3 solar cell performance depending on the CBD CdS annealing conditions

The evolution of the PV parameters of the CdS/Sb_2Se_3 solar cells are provided in Table 3.3. All the PV parameters are systematically decreasing with the increase of the CBD CdS annealing temperature. The devices with CBD CdS annealed at 200°C in air exhibit the highest efficiency of 2.8%, with a V_{oc} of 350mV, J_{sc} of 18.3mA/cm^2, and fill factor (FF) of 43%.

Table 3. 3 CdS/ Sb_2Se_3 solar cell device parameters with air and vacuum annealed CdS at 200-400°C.

Annealing Temperature	Ambient Conditions	V_{OC} [mV]	J_{SC} [mA/cm^2]	FF [%]	PCE/Eff [%]
As dep	---	230±10	13.7±0.5	39±1.5	1.2±0.2
150 °C	**Vacuum**	245±10	14.7±0.4	42±1.2	1.4±0.3
	Air	335±10	15.1	41±0.6	2.1±0.2
200 °C	**Vacuum**	260±10	16.4±1.2	44±2.4	1.8±0.2
	Air	350±10	18.3±0.9	43±1.1	2.8±0.2
250 °C	**Vacuum**	250±10	15.2±0.8	42±1.5	1.7±0.2
	Air	320±10	12.4±0.7	40±1.3	1.5±0.2
300 °C	**Vacuum**	215±10	13.6±0.8	39±1.1	1.1±0.2
	Air	290±15	7.6±2.3	38±2	0.8±0.2
350 °C	**Vacuum**	170±15	8.2±2.7	33±1.7	0.5±0.1
	Air	115±10	5.2±1.9	32±0.7	0.2±0.1
400 °C	**Vacuum**	110±15	6.5±0.9	33±0.6	0.2±0.05
	Air	90±20	3.7±2.3	29±1.8	0.1±0.07

There can be many reasons for this improvement but, the lowest concentration of oxygen–containing phases, larger grains of CdS, and fewer interface defects between the CdS buffer layer and Sb_2Se_3 absorber layer can be the main reasons as we studied earlier. The solar cell with vacuum annealed CdS films at 200 °C showed efficiency of 1.8 with V_{oc} of 260mV, J_{sc} of 16.4 mA/cm^2, and fill factor (FF) of 44% (Table 3.3). As annealing temperature increases PCE going down similarly, we discussed in section 3.1. In general, devices fabricated with CBD CdS annealed in air at low temperatures show better performances even though the air annealed CBD CdS illustrated lower bandgap values than in vacuum. J–V curves, as seen in figure 3.10 were measured to evaluate the effect of CdS annealing on the CdS/Sb_2Se_3 solar

cell performance. CBD CdS air annealed at 200°C provides a balanced environment with oxygen contain phases to intermixing and recrystallization of CdS/Sb_2Se_3 solar cell, securing the highest device performance.

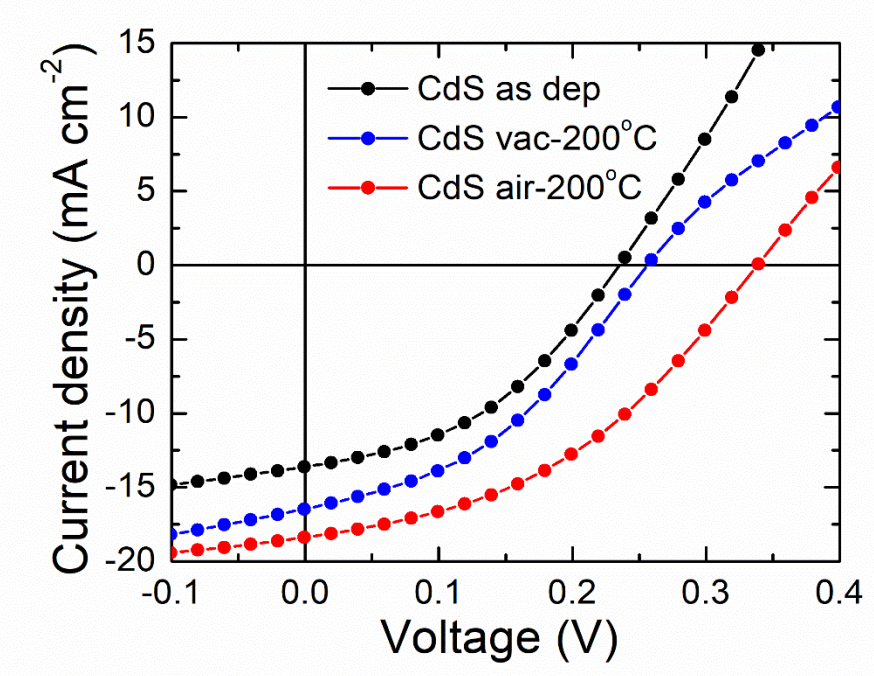

Figure 3. 10 J–V characteristic of CdS/ Sb_2Se_3solar cell with as deposited and annealed CdS in air and vacuum at 200°C

Overall, devices annealed in vacuum have low values for device efficiency, FF, short circuit current density, and open–circuit voltages. During the annealing process, will remove oxygen content from the grain boundaries, which allows for intermixing between the buffer layer and buffer layers.

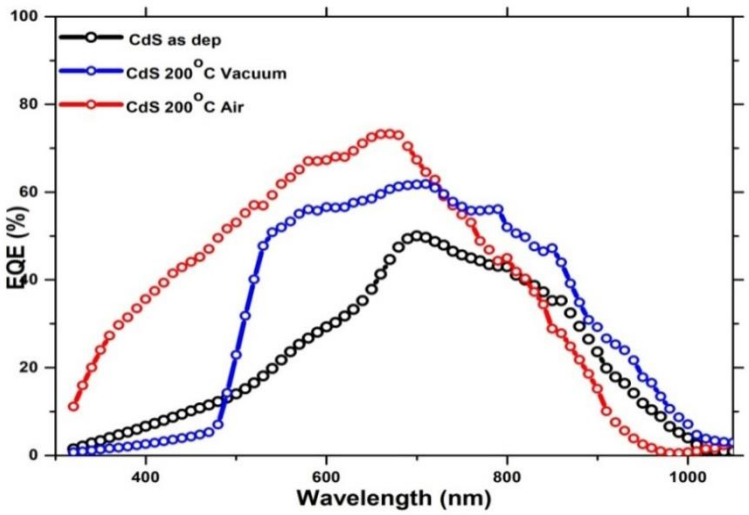

Figure 3. 11 EQE of glass/FTO/CdS/ Sb_2Se_3/Au solar cells with as deposited CBD CdS and annealed layers at 200□C in air and vacuum

External Quantum Efficiency of the Au/Sb_2Se_3/CdS/FTO/glass with CdS films annealed in vacuum and air at 200 ^oC are given in the figure 3.12. The device with the highest PCE, gained from CBD CdS annealed in air at 200^oC demonstrates the highest spectral response through the wavelength from 350–1000nm wavelength range. At shorter wavelengths (<500nm), the quantum efficiency improvement is trivial, pointing out that photo–excited carriers are accumulated efficiently when generated near the CdS/Sb_2Se_3 heterojunction. The reason is majority carrier holes have enough time to travel through the absorber layer to back contact. At wavelengths, (>500nm),EQE has a clear improvement indicating that the collection of the minority carriers' electron collection is the key drawback for the device performances[64]. In general, EQE indicates the device shows efficient carrier transport and better collection efficiency. The reason may be non–ideal behavior of other devices annealed at different air and vacuum temperatures because carriers have short diffusion length as result of recombination at the GBs.

CONCLUSIONS

CdS thin films were deposited by CBD technique and systematic investigation of the changes in the properties of the layers induced by post deposition vacuum and air annealing at 200-400 ^{o}C for 30 min was carried out. The annealed CdS films were applied as a buffer layer in Sb_2Se_3 thin film solar cells and their impact on the device performance was annualized.

The results are as follow:

1. Properties of CBD CdS and fabricated CdS/Sb_2Se_3 devices possess better properties at ambient temperatures of 200– 250 ^{0} C. When confined to electrical properties, the creation of shallow donors of Cl^{+}, OH^{+}, and acceptors Cd^{2-} demonstrates an n–type semiconductor.
2. CBD CdS shows higher electron density in air and vacuum at 250°C (1019 cm^{-3}). Electron density starts to drop exponentially due to the diffusion of Cd and other dopants to limit the kinetics.
3. The lattice parameter, interplanar distance, and main peak (111) shift illustrates that crystalline transformation from intermediate cubic–hexagonal to a stable cubic structure.
4. The main hypothesis of the thesis is the incorporation of hydroxide group during the process to the CdS lattice on the sulfur site creating a complex compound instead of CdS. Incorporated hydroxide group n sulfur site heavily affects the structural, optical, and electrical properties when thermal annealing is carried out.
5. When the annealing takes place hydroxide group decomposes into water resulting in cadmium oxysulfide solid solution and sulfur vacancies. At the same time, reduction of oxygen content in the sulfur site as thermally processing, the lattice configuration of CdS thin film converts to a stable cubic structure.
6. The bandgap of 2.42eV attributed to the incorporated $Cd(OH)_2$ immediately dropped as the annealing temperature increases.
7. From the performances of glass/FTO/Sb_2Se_3/CdS solar cell devices, it can conclude that the thermal annealing of buffer layer plays a significant role in improving the performance of the device and one of the key parameters in controlling the properties of CdS thin films.

REFERENCES

[1] R. Krautmann, "Faculty of Chemical and Materials Technology DEVELOPMENT OF Sb 2 Se 3 THIN FILM SOLAR CELLS BY CLOSE-SPACED SUBLIMATION Sb 2 Se 3 õhukese kile liste päikesepatareide arendamine lähidistants - sublimatsiooni meetodil Student :," 2019.

[2] "Part 2: Solar Energy Reaching The Earth's Surface | ITACA." https://www.itacanet.org/the-sun-as-a-source-of-energy/part-2-solar-energy-reaching-the-earths-surface/ (accessed May 07, 2021).

[3] F. Ise, "Photovoltaics Report." Accessed: May 07, 2021. [Online]. Available: www.ise.fraunhofer.de.

[4] L. Wang *et al.*, "Ambient CdCl2 treatment on CdS buffer layer for improved performance of Sb2Se3 thin film photovoltaics," *Appl. Phys. Lett.*, vol. 107, no. 14, p. 143902, Oct. 2015, doi: 10.1063/1.4932544.

[5] A. Romeo, D. L. Bätzner, H. Zogg, C. Vignali, and A. N. Tiwari, "Influence of CdS growth process on structural and photovoltaic properties of CdTe/CdS solar cells," *Sol. Energy Mater. Sol. Cells*, vol. 67, no. 1–4, pp. 311–321, 2001.

[6] "School of Engineering Department of Materials and Environmental Technology INFLUENCE OF pH ON THE PROPERTIES OF CHEMICALLY DEPOSITED CdS THIN FILMS AND SOLAR CELLS," 2017.

[7] R. K. Tamrakar, "Thermoluminescence studies of copper-doped cadmium sulphide nanoparticles with trap depth parameters," *Res. Chem. Intermed.*, vol. 39, no. 9, pp. 4239–4245, 2013.

[8] S. Lee *et al.*, "A transparent bending-insensitive pressure sensor," *Nat. Nanotechnol.*, vol. 11, no. 5, pp. 472–478, 2016.

[9] C. Wang, R. Cheng, L. Liao, and X. Duan, "High performance thin film electronics based on inorganic nanostructures and composites," *Nano Today*, vol. 8, no. 5, pp. 514–530, 2013.

[10] S. Mishra, A. Ingale, U. N. Roy, and A. Gupta, "Study of annealing-induced changes in CdS thin films using X-ray diffraction and Raman spectroscopy," *Thin Solid Films*, vol. 516, no. 1, pp. 91–98, 2007.

[11] U. Mishra and J. Singh, *Semiconductor device physics and design*. Springer Science & Business Media, 2007.

[12] H. A. Atwater and A. Polman, "Plasmonics for improved photovoltaic devices," *Mater. Sustain. energy A Collect. peer-reviewed Res. Rev. Artic. from Nat. Publ. Gr.*, pp. 1–11, 2011.

[13] K. N. Chopra and A. K. Maini, *Thin films and their applications in military and*

civil sectors. Defence Research and Development Organisation, Ministry of Defence, 2010.

[14] S. Mokrushin and Y. D. Tkachev, "EXPERIMENTAL INVESTIGATION OF LAMINAR SYSTEMS. 27. FORMATION OF ULTRATHIN CADMIUM SULFIDE LAYERS AT SOLUTION SOLID INTERFACE," *Kolloidn. ZHURNAL*, vol. 23, no. 4, p. 438, 1961.

[15] T. Negami, Y. Hashimoto, and S. Nishiwaki, "Cu (In, Ga) Se2 thin-film solar cells with an efficiency of 18%," *Sol. Energy Mater. Sol. Cells*, vol. 67, no. 1–4, pp. 331–335, 2001.

[16] M. Tsuji, T. Aramoto, H. Ohyama, T. Hibino, and K. Omura, "Characterization of CdS thin-film in high efficient CdS/CdTe solar cells," *Jpn. J. Appl. Phys.*, vol. 39, no. 7R, p. 3902, 2000.

[17] X. He, W. Liu, C. Zhu, and G. Jiang, "CdS Thin Films Deposited by CBD Method on Glass," vol. 24, no. 4, pp. 471–476, 2011, doi: 10.1088/1674-0068/24/04/471-476.

[18] O. Access, "We are IntechOpen , the world ' s leading publisher of Open Access books Built by scientists , for scientists TOP 1 %."

[19] N. Maticiuc, *Mechanism of Changes in the Properties of Chemically Deposited CdS Thin Films Induced by Thermal Annealing NATALIA MATICIUC*. .

[20] J. A. García-Valenzuela, "Simple thiourea hydrolysis or intermediate complex mechanism? Taking up the formation of metal sulfides from metal–thiourea alkaline solutions," *Comments Inorg. Chem.*, vol. 37, no. 2, pp. 99–115, 2017.

[21] R. Ortega-Borges and D. Lincot, "Mechanism of chemical bath deposition of cadmium sulfide thin films in the ammonia-thiourea system: in situ kinetic study and modelization," *J. Electrochem. Soc.*, vol. 140, no. 12, p. 3464, 1993.

[22] N. Amin and K. S. Rahman, "Close-Spaced Sublimation (CSS): A Low-Cost, High-Yield Deposition System for Cadmium Telluride (CdTe) Thin Film Solar Cells," *Mod. Technol. Creat. Thin-film Syst. Coatings*, vol. 361, 2017.

[23] C. Doroody *et al.*, "Temperature difference in close-spaced sublimation (CSS) growth of CdTe thin film on ultra-thin glass substrate," *Results Phys.*, vol. 18, p. 103213, Sep. 2020, doi: 10.1016/j.rinp.2020.103213.

[24] N. Spalatu, "Development of CdTe absorber layer for thin-film solar cells." Ph. D. Thesis, Tallinn University of Technology: Tallinn, Estonia, 2017.

[25] "(19) (PDF) Influence of CdS Layer on Texture Characteristics of CdTe Films Grown by CSS Combined with Substrate Rotation." https://www.researchgate.net/publication/275345485_Influence_of_CdS_Layer_on_Texture_Characteristics_of_CdTe_Films_Grown_by_CSS_Combined_with

_Substrate_Rotation (accessed May 09, 2021).

[26] X. Wen *et al.*, "Vapor transport deposition of antimony selenide thin film solar cells with 7.6% efficiency," *Nat. Commun.*, vol. 9, no. 1, pp. 1–10, 2018.

[27] F. Vázquez-Monroy, A. García-Barrientos, J. A. Hoyo-Montaño, G. Valencia-Palomo, H. Gómez-Pozos, and J. L. Bernal, "Fabrication and Characterization of CdS Thin Film Synthesized by CBD Deposited from pH-Controlled Growth Solutions for Solar Cells Applications," *Metallogr. Microstruct. Anal.*, vol. 5, no. 1, pp. 62–68, Feb. 2016, doi: 10.1007/s13632-015-0253-x.

[28] S. Adachi, *Properties of group-iv, iii-v and ii-vi semiconductors*, vol. 16. John Wiley & Sons, 2005.

[29] S. Route, "Study the Photocatalytic behavior of Nanocomposite CdS-TiO2 Synthesized by Sonochemical Route."

[30] A. L. Fahrenbruch, R. H. Bube, and R. V D'Aiello, "Fundamentals of Solar Cells (Photovoltaic Solar Energy Conversion)," 1984.

[31] D. Cha, S. Kim, and N. K. Huang, "Study on electrical properties of CdS films prepared by chemical pyrolysis deposition," *Mater. Sci. Eng. B*, vol. 106, no. 1, pp. 63–68, 2004.

[32] W. J. Danaher, L. E. Lyons, and G. C. Morris, "Some properties of thin films of chemically deposited cadmium sulphide," *Sol. Energy Mater.*, vol. 12, no. 2, pp. 137–148, 1985.

[33] X. Wu *et al.*, "Nanostructured CdS: O film: preparation, properties, and application," *Phys. status solidi*, vol. 1, no. 4, pp. 1062–1066, 2004.

[34] O. Vigil, O. Zelaya-Angel, and Y. Rodriguez, "Changes of the structural and optical properties of cubic CdS films on annealing in H2 and air atmospheres," *Semicond. Sci. Technol.*, vol. 15, no. 3, p. 259, 2000.

[35] K. Senthil, D. Mangalaraj, and S. K. Narayandass, "Structural and optical properties of CdS thin films," *Appl. Surf. Sci.*, vol. 169, pp. 476–479, 2001.

[36] B. E. McCandless, I. Youm, and R. W. Birkmire, "Optimization of vapor post-deposition processing for evaporated CdS/CdTe solar cells," *Prog. photovoltaics Res. Appl.*, vol. 7, no. 1, pp. 21–30, 1999.

[37] R. Kondrotas, C. Chen, and J. Tang, "Sb2S3 Solar Cells," *Joule*, vol. 2, no. 5, pp. 857–878, 2018, doi: 10.1016/j.joule.2018.04.003.

[38] Y. Zhou *et al.*, "Thin-film Sb 2 Se 3 photovoltaics with oriented one-dimensional ribbons and benign grain boundaries," *Nat. Photonics*, vol. 9, no. 6, pp. 409–415, 2015.

[39] S. Messina, M. T. S. Nair, and P. K. Nair, "Antimony selenide absorber thin films in all-chemically deposited solar cells," *J. Electrochem. Soc.*, vol. 156, no. 5, p. H327, 2009.

[40] L. Wang *et al.*, "Stable 6%-efficient Sb 2 Se 3 solar cells with a ZnO buffer layer," *Nat. Energy*, vol. 2, no. 4, pp. 1–9, 2017.

[41] C. Chen *et al.*, "6.5% certified efficiency Sb2Se3 solar cells using PbS colloidal quantum dot film as hole-transporting layer," *ACS Energy Lett.*, vol. 2, no. 9, pp. 2125–2132, 2017.

[42] O. S. Hutter, L. J. Phillips, K. Durose, and J. D. Major, "6.6% efficient antimony selenide solar cells using grain structure control and an organic contact layer," *Sol. Energy Mater. Sol. Cells*, vol. 188, pp. 177–181, 2018.

[43] L. J. Phillips *et al.*, "Current enhancement via a TiO2 buffer layer for CSS Sb2Se3 solar cells: performance limits and high V oc," *IEEE J. Photovoltaics*, vol. 9, no. 2, pp. 544–551, 2018.

[44] H. Shiel *et al.*, "Chemical etching of Sb2Se3 solar cells: surface chemistry and back contact behaviour," *J. Phys. Energy*, vol. 1, no. 4, p. 45001, 2019.

[45] C. Chen *et al.*, "Characterization of basic physical properties of Sb 2 Se 3 and its relevance for photovoltaics," *Front. Optoelectron.*, vol. 10, no. 1, pp. 18–30, 2017.

[46] "X-ray Powder Diffraction (XRD)." https://serc.carleton.edu/research_education/geochemsheets/techniques/XRD.html (accessed May 07, 2021).

[47] "InfoPage - Chemistry LibreTexts." https://chem.libretexts.org/Bookshelves/Analytical_Chemistry/Supplemental_Modules_(Analytical_Chemistry)/Instrumental_Analysis/Diffraction_Scattering_Techniques/00%3A_Front_Matter/02%3A_InfoPage (accessed May 07, 2021).

[48] D. Abou-Ras, T. Kirchartz, and U. Rau, *Advanced characterization techniques for thin film solar cells*, vol. 2. Wiley Online Library, 2011.

[49] "Scanning Electron Microscopy - Nanoscience Instruments." https://www.nanoscience.com/techniques/scanning-electron-microscopy/ (accessed May 07, 2021).

[50] mohammad reza Fadavieslam and S. Sadra, "Dependence of O2 and Ar2 flow rates on the physical properties of ATO thin films deposited by atmospheric pressure chemical vapor deposition (APCVD)," *Appl. Phys. A*, vol. 123, Oct. 2017, doi: 10.1007/s00339-017-1229-2.

[51] R. Zhang and B. Ulery, "Synthetic Vaccine Characterization and Design," *J. Bionanoscience*, vol. 12, pp. 1–11, Feb. 2018, doi: 10.1166/jbns.2018.1498.

[52] N. S. Kozhevnikova, A. A. Rempel, F. Hergert, and A. Magerl, "Structural study of the initial growth of nanocrystalline CdS thin films in a chemical bath," *Thin Solid Films*, vol. 517, no. 8, pp. 2586–2589, 2009.

[53] E. Technology, "I-V characteristics measurements of solar cells," 2019.

[54] N. Maticiuc, J. Hiie, T. Potlog, V. Valdna, and A. Gavrilov, "Influence of annealing in H2 atmosphere on the electrical properties of thin film CdS," *MRS Online Proc. Libr.*, vol. 1324, 2011.

[55] T. Potlog, "STRUCTURAL CHANGES IN CHEMICALLY DEPOSITED CdS: EFFECT OF THERMAL ANNEALING," 2010.

[56] J. Major, "Durham E-ThesesCdTe solar cells: growth phenomena and device performance," pp. 1–249, 2008, [Online]. Available: http://ethos.bl.uk/OrderDetails.do?uin=uk.bl.ethos.505146%5Cnpapers2://publication/uuid/5B398D3F-E5F9-4236-A92A-AFE7D1C2DF98.

[57] "plasticphotovoltaics.org." http://ww12.plasticphotovoltaics.org/ (accessed May 07, 2021).

[58] "Quantum Efficiency | PVEducation." https://www.pveducation.org/pvcdrom/solar-cell-operation/quantum-efficiency (accessed May 18, 2021).

[59] X. Yang, C. Xu, and N. C. Giles, "Intrinsic electron mobilities in CdSe, CdS, ZnO, and ZnS and their use in analysis of temperature-dependent Hall measurements," *J. Appl. Phys.*, vol. 104, no. 7, 2008, doi: 10.1063/1.2996032.

[60] H. Kim *et al.*, "Electrical, optical, and structural properties of indium-tin-oxide thin films for organic light-emitting devices," *J. Appl. Phys.*, vol. 86, no. 11, pp. 6451–6461, 1999, doi: 10.1063/1.371708.

[61] J. Maricheva, S. Bereznev, R. Naidu, N. Maticiuc, V. Mikli, and J. Kois, "Improved electrodeposition of CdS layers in presence of activating H2SeO3 microadditive," *Mater. Sci. Semicond. Process.*, vol. 54, pp. 14–19, 2016.

[62] W. Li, X. Cai, Q. Chen, and Z. Zhou, "Influence of growth process on the structural, optical and electrical properties of CBD-CdS films," *Mater. Lett.*, vol. 59, no. 1, pp. 1–5, 2005, doi: 10.1016/j.matlet.2004.04.008.

[63] N. Maticiuc, J. Hiie, V. Mikli, T. Potlog, and V. Valdna, "Structural and optical properties of cadmium sulfide thin films modified by hydrogen annealing," *Mater. Sci. Semicond. Process.*, vol. 26, pp. 169–174, 2014.

[64] D. B. Li *et al.*, "Stable and efficient CdS/Sb2Se3 solar cells prepared by scalable close space sublimation," *Nano Energy*, vol. 49, no. March, pp. 346–353, 2018, doi: 10.1016/j.nanoen.2018.04.044.